Review Article

Ultrafast Devices Based on Surface Plasmons on Bulk Metal and Graphene: Switches, Modulators, and Microscope Electron Sources

Jing Zhao⬤, Jianlong Liu, Ruirui Jiang, Kaiqiang Yang, and Baoqing Zeng*

School of Electronic Science and Engineering, University of Electronic Science and Technology of China, Chengdu 610054, China

Optical modulation and switch are crucial in photonics technologies, and microscope electron sources are essential in imaging. However, it is an obstacle to integrating those devices with conventional techniques. Moreover, they cannot function in ultrafast communication and signal processing systems. The surface plasmon resonance phenomenon is of wide interest due to its abundant physics, such as the local field enhancement enabling strong light-matter interactions, breaking the diffraction limit to realize subwavelength structures, and going beyond the speed limit intrinsic to conventional semiconductor materials and devices. Here, by reviewing the various advantages of surface plasmons in different nanostructures or materials, we intend to propose the development trend and designed configuration of such ultrafast devices (usually induced by ultrafast laser) such as modulators, switches, and microscope electron sources. Based on the surface plasmons, ultrafast devices will tend to be more energy-efficient, low-energy consumption, and miniature. We also envision the development of surface plasmons with alternative materials or structures. This review will facilitate the development of ultrafast devices.

I. INTRODUCTION

Over the past few decades, the development of ultrafast science has been a major research hotspot, and diverse ultrafast devices have received attention in physics, materials science, and nanotechnology. There are some reasons. On the one hand, as ultrashort pulsed lasers leap from femtoseconds to attoseconds (1 attosecond $= 10^{-18}$ s), and attoseconds endow ultrashort with more meanings [1]. On the other hand, the advance to understanding the fundamental processes in matter is determined by the ability to investigate ultrafast phenomena at shorter and shorter temporal scales [2]. The topics of ultrafast science involve but are not limited to attosecond light sources [3], attosecond physics [4], ultrafast modulators [5], ultrafast imaging [6], ultrafast electron sources [7], and other ultrafast phenomena [8,9]. With the rapid development of optical techniques, material micromachining technology, and integrated optical component technology, data-transmission systems and imaging systems require highly increasing integration and miniaturization of ultrafast photonic devices. Moreover, compared with general electronic devices, photonic devices have the advantages of high bandwidth, high density, high speed, and low-energy consumption [10], which can lead us into an era of all-optical integration, meeting the requirements of ultrafast device development.

However, photonic devices meet a bottleneck in pursuing ultracompact optical devices due to Abbe's diffraction limit in conventional photonics [11]. How to obtain the high-efficiency optical devices (such as optical couplers, optical switches, electron sources, and optical modulators) that break through the diffraction limit is the cornerstone for realizing nanometer all-optical integration. Higher requirements are put forward for the development of alternative devices in the future: for one thing, the size of optical devices is required to be highly miniaturized, which is convenient for nanoapplication and high-density integration. For another thing, it is required to be able to characterize and control the light field at the nanoscale, and realize focusing, transformation, coupling, refraction, conduction, and multiplexing at the nanoscale. Therefore, other light sources that achieve high collimation and superdiffraction and various nanophotonics devices emerge [12–19].

In recent years, researchers have suggested surface plasmon-based structures and devices to offer an opportunity to develop ultracompact nanometallic devices [20,21]. Plasmonic topological insulators can be compatible with integrated photoelectric systems to manipulate light at nanosecond-level switching time [22]. That is because surface plasmons are the electronic resonance generated at the metal-dielectric interface by the interaction of light and metal-free electrons [23], which can overcome the diffraction limit. Due to the unique properties of subwavelength localization and local near-field enhancement, ultrafast surface plasmons excited by

*bqzeng@uestc.edu.cn

femtosecond laser enable us to manipulate and control photons on the femtosecond time and nanospace scales [24], which are better than previous works with subsecond corresponding times with submicrosecond or nanosecond response times [25,26]. Surface plasmons have received increasing interest in optical computing [27], nanointegrated photonics [28], optical imaging [29], biosensing [30], optical modulator [31], solar cells [32], and surface-enhanced Raman spectroscopy [33], etc. Surface plasmon-based applications provide an opportunity for integrating conventional photonic devices on the same chip, or it enables photoelectron emission induced by plasmon at a much lower light intensity than usual [34].

This paper reviews the classification, structures, and applications of surface plasmon. And is organized as follows: Sec. II discusses two kinds of surface plasmon, involving their propagation behavior and a remarkably enhanced optical near field based on surface plasmons (SPs), which is beneficial for electron emission. Surface plasmons in three-dimensional (3D) metals and two-dimensional (2D) graphene are reviewed in Sec. III, including the introduction of graphene plasmon characteristics, which have advantages in the application of ultrafast devices. Based on the multiple nanostructures, surface plasmons are used in various devices, and the field-enhancement factors of typical structures are summarized in Sec. IV. Based on the exploration of SP, some ultrafast devices of SP are introduced in Sec. V, such as modulator, switch, and microscope electron source. Brief conclusions and an outlook of those ultrafast devices are given in the final section.

II. DIFFERENT SURFACE PLASMONS

Collective oscillations of free electrons under the excitation of the incident wave, gathered on the interface between a conducting material and the dielectric environment, are known as surface plasmons [23], which are an evanescent wave where the fields are highest at the interface and their amplitudes decay exponentially away from the interface. Benefiting from its strongly confined and enhanced electromagnetic fields, with fast dynamics lasting tens of femtoseconds, surface plasmons become the perfect tool in fast optical devices or processes, such as ultrafast optical switching, modulator, and electron-source-based–electron emission [35].

Based on different forms of free-electron oscillation under optical excitation, surface plasmon can be divided into localized surface plasmon resonance (LSPR) and surface plasmon polaritons (SPPs).

A. Localized surface plasmons

LSPR is the nonpropagating excitation of electrons coupled to electromagnetic fields, an oscillation of free electrons in a tiny particle. The plasma frequency is adjusted
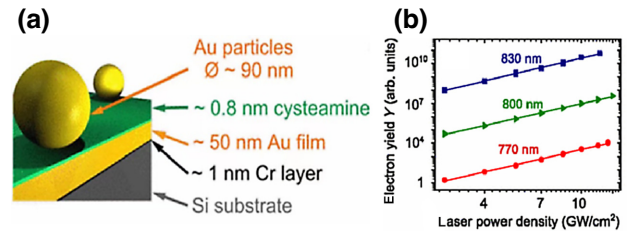

FIG. 1. (a) Sample structure. (b) Total electron yield versus laser power density [37].

by the size and shape of the particle, which decides the resonance frequency change. The device's simplest design consists of randomly distributed gold nanoparticles [36]. Metallic nanostructures also can support LSPR. Localized plasmons of different structures may lead to considerable field enhancement [37]. Plasmons are excited at Au nanoparticles with a diameter of 90 nm, which are in subnanometer distance to a 50-nm-thick Au film with an enhancement factor of 10^3 by femtosecond laser in the wavelength range of 750–850 nm [37] [see Fig. 1(a)].

1. Ultrafast electron emission methodology

Field electron emission is in the form of quantum tunneling of electrons through a potential barrier rather than across the potential barrier to a vacuum [see Fig. 2(b)]. A common methodology for optimizing the emitter is decreasing the work function Φ or increasing the field enhancement β, which is obtained according to the form described below. In field-emission methodology, the relationship between current density J and electric field intensity E is commonly called the Fowler-Nordheim (FN) formula [7]:

$$ J = \frac{e^3(\beta E)^2}{8\pi h \Phi} \exp\left[-\frac{8\pi\sqrt{2m}\Phi^{3/2}}{3he\beta E} \right], \quad (1) $$

h stands for the Planck constant, and the charge and mass of an electron are denoted by e and m, respectively.

Electric field emission assisted by an ultrafast laser can improve the performance of the original electron emission and then achieve ultrafast electron emission [38,39].
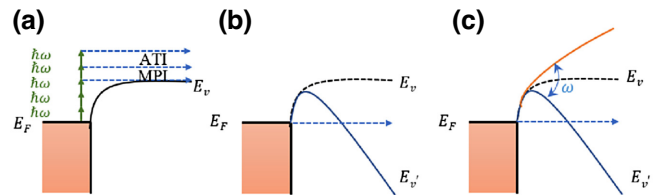

FIG. 2. (a) Multiphoton and above-threshold ionization (MPI and ATI); (b) field electron emission; (c) optical field emission (OFE).

The electron photoemission induced by high-intensity laser irradiation may transition into strong-field tunneling [40] from multiphoton ionization [40,41] (MPI) (involving the above-threshold ionization) [as shown in Figs. 2(a) and 2(c)]. The criterion is described by the Keldysh framework [42]. The Keldysh parameter is given by $\gamma = \omega\sqrt{2m_e\phi}/e\beta F$, where ω is the angular frequency, Φ is the work function, m_e is the electron rest mass, e is the elementary charge, β is the field-enhancement factor, and F is the peak electric field strength. There are two limiting regimes separated by the parameter: a multiphoton photoemission regime ($\gamma > 1$) and a tunneling emission regime ($\gamma < 1$). The latter is similar to field electron emission, a type of electron tunneling emission, termed optical field emission (OFE).

OFE is a photoemission regime, even requiring the intensity on the order of TW cm^{-2} (in the IR range). Electrons from states near the Fermi level can tunnel through the narrow barrier during a fraction of the negative half-optical cycle in the course of strong-field photoemission where the surface vacuum level varies periodically with a sufficient strong optical field.

Some studies on methods of ultrafast electron emission combine field electron emission and optical field emission [38,43,44]. And increase the β by surface plasmon.

2. Electron emission at low power density based on localized plasmons

Typically, photoemission is incited by laser intensities on the order of 1 TW cm^{-2} in the IR range without any field enhancement [44]. However, for reducing the power density of the laser, ultrafast electron emission can be achieved by increasing the field enhancement of emitters.

For 0.125-mm diameter tungsten single-crystal wire, the plasmon enhancements are too weak to be considered. Its radius of curvature is $r < \lambda/5$, and the field enhancement due to geometry is approximately 5 [45]. Electron emission is incited by high voltage and power density of laser at relatively weak enhancement. The bias voltage applied in the experiment exceeds 1000 V with 3×10^{10} W cm^{-2} of the peak intensity of the optical field in a tip (when the power of laser $P = 260$ mW). Photocurrent reaches the order of femtoampere when illuminated at 800-nm wavelength [as plotted in Figs. 3(a) and 3(b)] [38].

The enhancement factor is $\alpha \approx 10$ increased by using gold or tungsten to make metal tips with a radius of curvature of around 20 nm [43]. The electrons are generated from single-photon-assisted tunneling at high bias [38]. However, under 800-nm wavelength illumination with power on the order of milliwatts, the generation mechanism changed to four-photon induced emission at 0–1000 V bias voltage, enabling the emission of electrons at lower bias than before with the laser of sub-10-fs duration [see Fig. 3(c)].
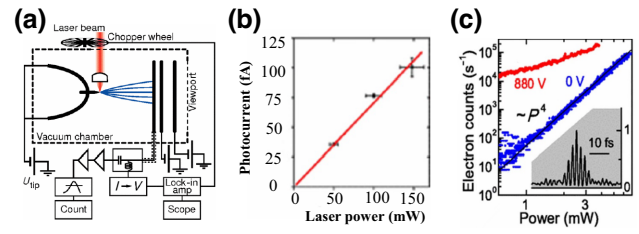

FIG. 3. (a) Experimental configuration. All equipment is installed in an ultrahigh vacuum chamber. Field emission electrons are emitted from the tip and accelerated onto the microchannel plate detector (MCP), which is located 4 cm away from the tip. (b) The photocurrent varies linearly with power [38]. (c) It exhibits a fourth-order power dependence (four photons absorbed) at zero bias [43]; at 880 V, the electron flux $I \propto P^{1.4}$ and $P = 3$ mW.

Considering the strong field enhancement of LSP, the field enhancement factor is 10^3 based on strongly coupled plasmons on gold nanoparticles at subnanometer distances from the gold film [37]. And a corresponding electric field strength is $E_{\text{laser}} \approx 50$ MV/m by illuminating nanoparticles with a power density of 6×10^8 W cm^{-2}. Therefore, the electric field strength between the nanoparticle and plane is $E_{\text{laser}} \approx 50$ GV/m [see Fig. 1(b)]. Field emission of electrons is generated without the help of a noticeable dc field in the 750–850 nm wavelength range.

If plasmon is introduced, electron emission can be achieved by applying the laser on the order of 1 GW cm^{-2} in the mid-IR by taking advantage of the local field enhancement properties of plasmons [37,46], and further studies showed that lower light intensity is enough for photoemission [44].

In their design, the structure consists of parallel gold ribbon arrays and a set of mushroomlike gold nanostructure arrays with a minimum gap size of 100 nm [see Fig. 4(a)]. Unprecedently, the electron emission is controlled by low bias voltages below 10 V and low power lasers (in IR),
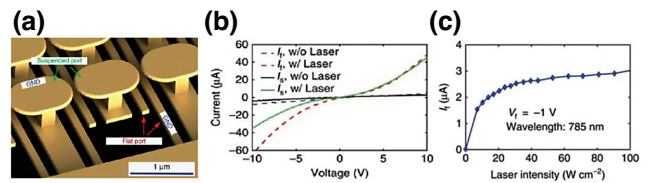

FIG. 4. (a) The designed photoemission-based device. V_f and V_s represent the voltage of the flat port and suspended port, respectively. Emission electrons can be manipulated by adjusting the voltage at the ports. (b) I-V curves of the suspended port when the flat port is open circuited. Similarly, the current of a flat port is a function of the voltage when the suspended port is open circuited (without or with laser: $I = 5$ W cm^{-2}). (c) The current of the flat port I_f is changed by the laser on the order of W cm^{-2} with the bias voltage of $V_f = 1$ V, while the suspended port is an open state [44].
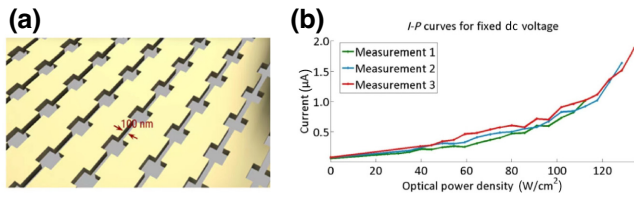
FIG. 5. (a) Plasmon-induced photoemission vacuum-channel device and the gap between cathode and anode is 100 nm. (b) Current versus optical power density [47].

which power is a few milliwatts with intensities of around 1 W cm^{-2} at the resonant wavelength (785 nm) [44] [as depicted in Fig. 4(b)].

There are some similar works following. Shiva Piltan *et al.* optimized a resonant metal array of multiple rows of gold elements [47]. The current in the order of µA was measured when irradiated by the laser with the intensity of W cm^{-2} for no more than 10 s [see Fig. 5]. Afterwards, Philipp Zimmermann *et al.* [48] designed and fabricated an interdigitated electrode consisting of a rhombus emitter and a planar collector [as shown in Fig. 6(a)]. Their experiments measure from −3 to 3 pA currents when the laser pulse energy is 405 pJ, and the bias voltage is from −0.5 to 0.5 V [see Fig. 6(c)]. This simultaneously demonstrates a unipolar electron current by designing the structure that can excite the plasmon to be asymmetric. As the laser intensity increases, the electron emission mechanism can be tuned from five-photon absorption toward tunneling (strong-field) photoemission for a barrier height of gold $\Phi_{\text{barrier}} \approx 5.1$ eV and a laser energy $\hbar\omega_{\text{laser}} \approx 1$ eV [as plotted in Fig. 6(b)].

Electron unipolar emission in the vacuum channel with hundreds of nanometers is realized by combining plasmon and the tip effect of nanostructure geometry, which can enhance the electric field at the emission point. Ultrafast
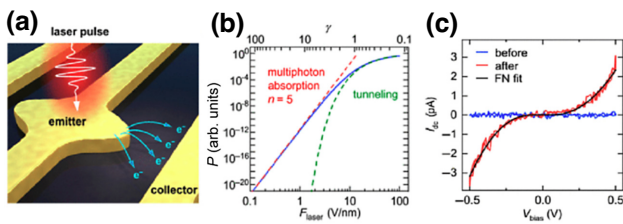

FIG. 6. (a) Sketch of an asymmetrical metal nanostructure with emission electron excited by a femtosecond laser pulse. (b) The curve of the electron emission versus F_{laser} is displayed in a blue line according to the Keldysh theory. Moreover, the Keldysh parameter γ is shown on the top axis. The red dashed line means multiphoton absorption for a low F_{laser}, whereas tunneling for a high F_{laser} is indicated by a green dashed line. (c) Three curves are I_{dc} versus V_{bias}. The blue is measured before laser illumination and after laser illumination can be drawn with a red curve fitted with a Fowler-Nordheim fit in black [48].

emission of electrons will be accomplished at a lower intensity of optical field emission with low dc bias voltage. The coplanar structure of the emitter and collector is conducive to integration. The regulation of current is realized due to the control of electron emission induced by light.

B. Surface plasmon polaritons and propagating surface plasmon

SPPs are polarized waves that propagate along a dielectric-metal interface, forming an evanescent field perpendicular to the interface, and the field amplitude decays exponentially away from the metal surface [49]. Due to the Ohmic effect along the metal surface, it can only travel a limited distance, and metals such as silver and gold with high conductivity and reflectivity have losses in the near- and midinfrared regions [23,50]. Therefore, the electromagnetic energy of SPPs is strongly confined near the surface, which has a large near-field enhancement effect.

1. Electron tunneling based on surface plasmon polaritons under low-power density

Surface plasmon polarization modes can be excited by coupling a light beam to a periodic metallic thin film (or metal grating) or a prism (including two configurations—Otto and Kretschmann) [34,46,51]. The metal layer is placed under the prism, which is the former configuration when there is a gap in the middle; otherwise, it is the latter model. The characteristics of the SP are sensitive to the refractive index in the metal-film surface, such as the resonant wavelength, intensity, or phase. Furthermore, the change in the refractive index depends on the concentration and properties of the biomolecules. Therefore, the Kretschmann configuration is often used in the applications of SPP-based optical biosensors. [52–55]. Similar to localized plasmons, high-field emission at low intensities can be realized with SPPs [46].

The pulse is focused on a right-angled edge of the CAF$_2$ prism and generates propagating surface plasmon along a 15-nm-thick gold film covering the hypotenuse of the prism [37,46] [see Fig. 7(a)]. According to the curves of focused laser intensity dependent of the total plasmonic photocurrent, there is a substantial change that the local slopes of the curves are drastically reduced when the focused intensity is around 0.6 W cm^{-2} [see Fig. 7(b)], which is the signature of the photoemission mechanism changing into tunneling [see Figs. 4(c) and 7(b)] [34,41, 56]. This change is due to the strong interaction of light and matter enhanced by propagating surface plasmon.

2. Nanofocusing of optical energy utilizing surface plasmon polaritons

Such evanescent waves at the interface also have the advantage of being propagative, which is beneficial for
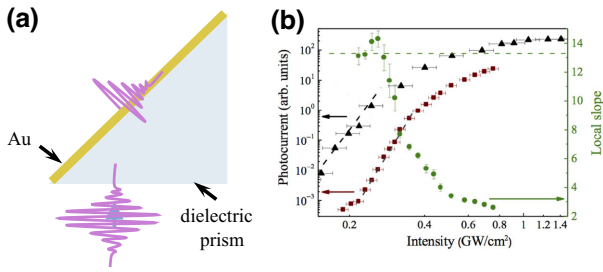
FIG. 7. (a) Structure of coupled plasmons with right-angle prism. (b) Functions of the total plasmonic photocurrent about focused laser intensity [spot sizes (FWHM) of 870 μm (black triangles) and 1400 μm (red squares) are two independent exemplary scans]. The local slope of the second curve is also plotted (green circles) [46].

propagating the energy of light-matter interactions forward. SPPs are tightly bound to the interface, which penetrates at approximately 100 nm in dielectric and approximately 10 nm in metal. The SPP field is strongly confined in the cross section, which is perpendicular to the SPP propagation direction, ensuring the feature that implies high densities of energy in the cross section [13] [see Fig. 8].

The propagation of SPP is suggested that can concentrate the energy in the tip early in 1999 [57]. The plasmon wave packet decreases as the cone or wedge radius decreases, and the wavelength decreases, wave fields grow, As described in Ref. [50]: $k = \eta/r$ (k is the wave number of the surface polariton [58], η is the separation constant to be determined from the boundary conditions, r is the distance to the apex of the tip). During the propagation of surface polarons through the cone- or wedge-shaped structure, the localization of the wave is in a very small spatial region and anomalous amplification of the electric field is realized by focusing light to subwavelength dimensions (approximately 20 nm in size) [59] [as shown in Fig. 9(a)]. In order to achieve 10-nm spatial resolution and few-femtosecond space resolution, Samuel Berweger *et al.* took advantage of the gratings to combine it with a conical
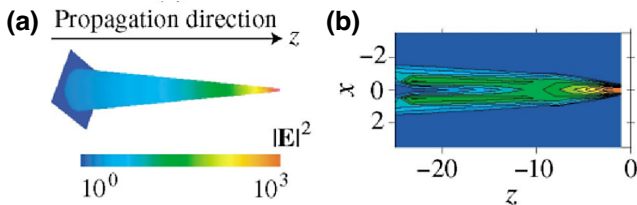

FIG. 8. (a) Geometry of the nanoplasmonic waveguide. Relative to the excitation fields, $I(r) = |E(r)|^2$ demonstrates the intensity of the local fields. (b) The vertical cross-section electric field of the waveguide. The radius of the waveguide gradually decreases from 50 to 2 nm along the propagation direction of the SPP [13].
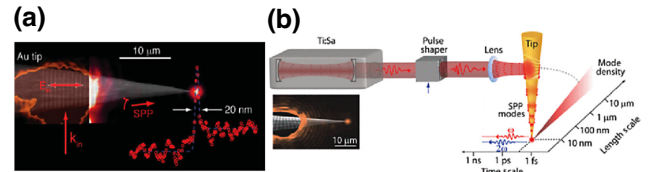

FIG. 9. (a) Evanescent plasmon propagation along the taper and energy focus at the tip with 4–10-nm radius [59]. (b) SPPs generated by grating-coupled femtosecond pulses condense adiabatic fields into nanoscale apex volumes [60]. SEM and optical image of a tip with a broadband grating (bottom left).

noble metal tip [60] [see Fig. 9(b)]. Another idea for ultrafast electron sources is provided by keeping relatively low propagation losses and focusing the energy of light into the nanoscale range [61,62].

III. SP IN DIFFERENT MATERIALS

When it comes to plasmons, metals are the common material. However, especially in the range of visible light and ultraviolet spectrum, large losses of those metals due to plenty of free electrons seriously limit the practicality of some current plasmonic devices [63–65]. Moreover, the losses are the inherent nature of the materials [66]. So it is necessary to find alternative plasmonic materials with lower losses, which can develop alternative plasmonic devices, while fully exploiting materials' natural advantages [67].

Plasmons exhibit different properties based on various materials and structures. Other materials have been extended by researchers in their works besides noble metals. Metals, semiconductors, and two-dimensional materials can cover a wide spectrum from ultraviolet, visible, near infrared to far infrared by using diverse morphologies and structures [68].

A. SP in metal

The Drude or free-electron model is the simplest model for the dielectric constant of a metal to describe dc conductivity in metals [69]. The Drude model as the expression for the dielectric constant can be described as

$$\epsilon(\omega) = 1 - \frac{\omega_p^2}{\omega(\omega + i/\tau)}, \qquad (2)$$

where $1/\tau$ is the damping constant, and ω_p describes the plasma frequency for most metals, $1/\tau$ is much less than ω_p, and the plasma frequency for metals is usually in the visible regions at room temperature [70]. Therefore, the conduction electrons of metals under light excitation are confined to dimensions comparable to or smaller than the wavelength of light, which can result in LSPR. If the
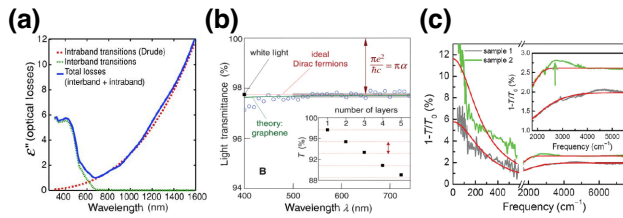
FIG. 10. (a) Imaginary permittivity or optical losses in gold [63,66]. (b) Transmittance spectrum of single-layer graphene as a function of wavelength (open circles). [Inset: the number of graphene layers dependent on transmittance of white light (squares)] [73]. (c) Infrared absorption spectra of epitaxial graphene. (Inset: locally enlarged view of the mid-IR absorption curves) [74].
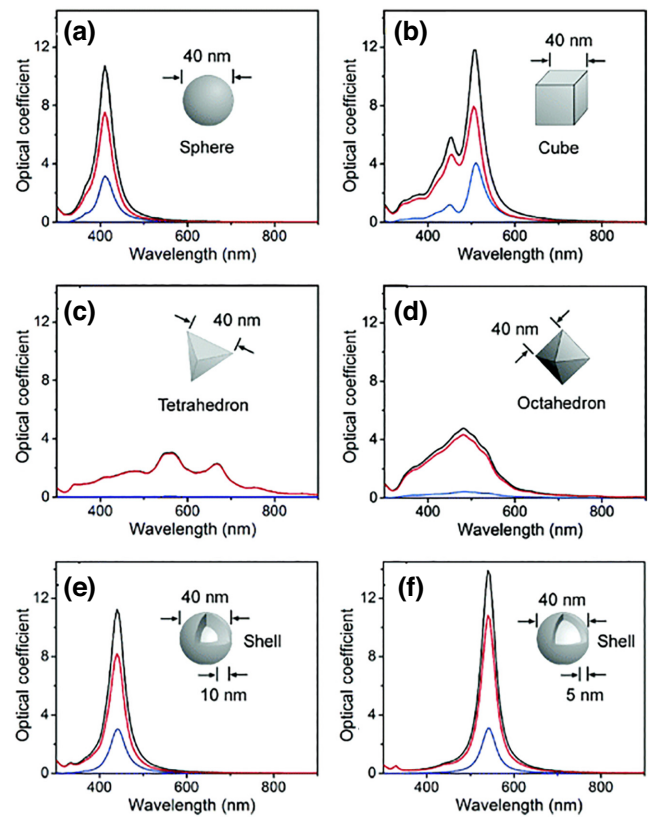

FIG. 11. (a) Calculated curves of extinction (black), absorption (red), and scattering (blue) spectra of silver nanostructure (note: extinction = absorption + scattering). The shape of the nanostructure is respectively an isotropic sphere in (a), an anisotropic cube in (b), a tetrahedron in (c), an octahedra in (d), a hollow sphere in (e) and a thinner shell in (f) [77].

interaction of field control extends to metallic nanostructures supporting LSPR, strong field light-matter interactions can be studied in chip scale [71] with lower power of the exciting light [44]. LSPR with interesting optical properties are attractive for various applications. Ultrafast electron sources are pushed to higher temporal and spatial resolution by combining plasmons. [72].

Metals with high conductivity are popularly assumed to be excellent candidates when applied to plasmonic applications [66]. Among them, gold is the most stable, so it is widely used for stimulating plasmonics. Because gold and silver have a relatively low loss in the visible range, they have become the two most commonly used materials for plasmonic applications. However, silver is easier to oxidize than gold in practice. The two interband and intraband losses are determined by the imaginary part of the permittivity. The Drude losses (intraband losses) in gold are high (in NIR), though they are lower for shorter wavelengths [as displayed in Fig. 10(a)]. Moreover, interband transitions in metals such as gold are high in the visible range, which makes the search for more plasmonic materials necessary. In other words, the metals can be kept by using patterned apertures on their surfaces, which are named spoof surface plasmon [75].

Both intrinsic properties of material and extrinsic properties (such as free carrier concentration, size, and shape) can affect the resonant frequency and the field enhancement [76]. The geometric morphologies of metallic nanoparticles and nanostructures are harnessed to explore the shaping and manipulating of plasmonic properties [77] [as plotted in Fig. 11]. The surface polarization (charge separation) will be changed by particle size or shape variation, and thus the resonance peak changes. It also benefits from metallic nanostructures that are easy to grow and do not require fine processing [37,71,78,79]. Silver and gold films or nanoparticles and metal-coated nanoparticles can be fabricated through existing technology. The former are various physical vapor deposition (PVD) techniques. The latter is the synthesis of liquid chemical methods [80].

Electron-beam and thermal evaporation and sputtering are the two main types of PVD methods [66].

B. SP in graphene

2D materials with atomic scale thickness have the property that high field enhancement at their edges due to an extremely high aspect ratio.

Graphene, representative of two-dimensional materials, has recently become a popular plasmonic material and shows lots of extraordinary electrical and optical properties [81]. The density's dependence of the plasma frequency of two-dimensional graphene ($\omega_0 \propto n^{1/4}$) is different from that of general 2D electron gas ($\omega_0 \propto n^{1/2}$). The dielectric function of graphene can be calculated from the Lindhard formula: $\epsilon(\mathbf{q}, \omega) = 1 - (2\pi e^2/q) \chi(\mathbf{q}, \omega)$. The function $\chi(\mathbf{q}, \omega)$ is usually referred to as the "Lindhard function" and $\epsilon(\mathbf{q}, \omega)$ is the random-phase approximation (RPA) dynamical dielectric function where wave vector is $\mathbf{q}$ and frequency is ω [82–84].

Notably, the optical properties in graphene can be effectively controlled by tuning the Fermi energy [85,86],

such as favoring strong broadband light-matter interactions, which makes it beneficial for various optical modulations [87,88]. With electrically tunable, graphene can show plasmonic feature varying from midinfrared to terahertz for achieving functionalities in the broadband range [89,90]. In addition to the linear optical response, graphene also exhibits strong nonlinearity [91], including saturable absorption [92], and Kerr effect [93] in the near-infrared and visible spectral range. Graphene with those optical properties becomes a popular 2D material for optical devices. For example, based graphene fast saturable absorbers occupy a place in generating ultrafast optical pulses [94,95]. Three kinds of optical properties of graphene are described for the advantages of ultrafast devices based on graphene as follows.

1. Broadband light absorption

Intrinsic graphene, with only one atom thick can absorb a fraction ($\pi\alpha = 2.3\%$) of normal incident light in the range of 400–700 nm, and the rest of them are transmitted [73,96], [as depicted in Fig. 10(b)]. This result agrees with the Fresnel equations in the thin-film limit, which can describe the light absorption properties of graphene [97].

$$T = \frac{1}{(1 + 0.5\pi\alpha)^2} \approx 1 - \pi\alpha = 0.977. \quad (3)$$

The fine-structure constant is shown as $\alpha = e^2/\hbar c$ (c is the speed of light). The reflectivity ($R = \frac{1}{4}\pi^2\alpha^2 T$) is small and can be ignored. However, Hugen Yan *et al.* studied epitaxial graphene, and the reduction of transmission in that atomically thin film approaches 40% in the far-infrared light region; correspondingly, the infrared absorption rate will be increased to 12% [74] [see Fig. 10(b)].

In general, the resonant effect is an effective method to improve the interaction of light and matter, which can enhance the absorption or emission of materials [98,99]. The surface plasmon oscillation of some periodic metal structures can bind light on the surface, while graphene is now one layer of atomic thickness, which can fully contact the plasmon oscillation structure mentioned above. Therefore, metal nanostructures combined with graphene can utilize the light energy that is bound on the surface to improve the absorption of light. The absorption rate reaches even as high as 90% in the communication band region by coupling monolayer graphene with subwavelength grating on the top of the gold mirror [100] [as displayed in Fig. 12].

2. Carrier interband and intraband transition and ultrafast relaxation process

The absorption of the optical field is affected by the carrier concentration tuned by the applied bias voltage. Two steps about light absorption exist: the interband transitions dominated at high photon energies, while intraband
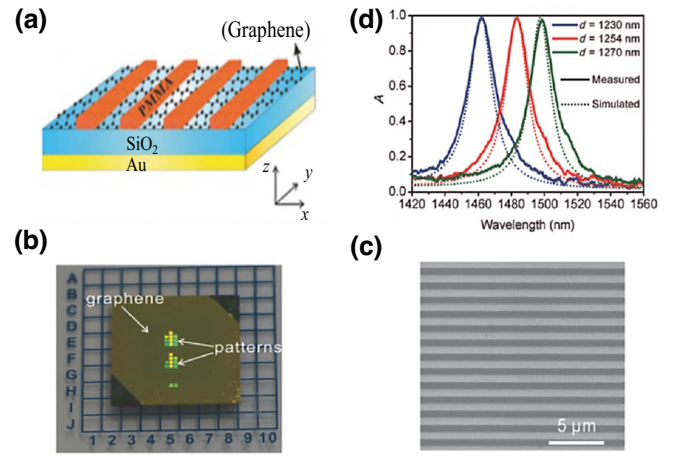

FIG. 12. (a) Schematic image of the absorption structure with monolayer graphene and subwavelength grating. (b) Optical image of the designed sample. (c) SEM image of the top pattern of a fabricated sample. (d) Measured (solid line) and simulated (dot line) absorption spectra of the fabricated sample with different grating periods d for TE polarization [100].

transitions at lower photon energies. A dynamic conductivity model can explain the involved processes. The simple model includes intraband and interband absorption [96,101].

$$\sigma(\omega, \mu_c, \Gamma, T) = \sigma_{\text{intra}} + \sigma_{\text{inter}},$$

$$\sigma_{\text{intra}} = \frac{ie^2}{\pi\hbar^2(\omega - j2\Gamma)} \int_0^\infty \xi \left(\frac{\partial f_d(\xi, \mu_c, T)}{\partial\xi} \right.$$
$$\left. - \frac{\partial f_d(-\xi, \mu_c, T)}{\partial\xi} \right) d\xi,$$

$$\sigma_{\text{intra}} = \frac{ie^2(\omega - j2\Gamma)}{\pi\hbar^2}$$
$$\times \int_0^\infty \frac{f_d(-\xi, \mu_c, T) - f_d(\xi, \mu_c, T)}{(\omega - j2\Gamma)^2 - 4(\xi/\hbar)^2} d\xi,$$

$$f_d(\xi, \mu_c, T) = (e^{(\xi - \mu_c)/k_B T} + 1)^{-1}. \quad (4)$$

The complex conductivity $\sigma(\omega, \mu_c, \Gamma, T)$ is affected by the angular frequency ω, the chemical potential μ_c, the charge particle scattering rate $2\Gamma = \tau^{-1}$ (where τ is the relaxation time), and Kelvin temperature T, $\hbar$, k_B, e, ξ, $f_d(\xi, \mu_c, T)$ are the reduced Planck constant, Boltzmann constant, electron charge, electron energy, and Fermi-Dirac distribution function, respectively.

Based on the semiclassical model under low-temperature and high-doping conditions, the conductivity of graphene

is usually calculated by the Kubo formula [102]:

$$\sigma = \sigma_{\text{intra}} + \sigma_{\text{inter}}$$

$$= \frac{e^2 \mu_c}{\pi \hbar^2} \frac{i}{(\omega + i\tau^{-1})} + \frac{e^2}{\pi \hbar^2} \left[\theta(\hbar\omega - 2|\mu_c|) \right.$$

$$\left. + \frac{i}{\pi} \ln \left| \frac{\hbar\omega - 2|\mu_c|}{\hbar\omega + 2|\mu_c|} \right| \right], \qquad (5)$$

where $\theta(\hbar\omega - 2|\mu_c|)$ is the step function.

The Fermi level is E_F, and the electrons that can undergo transitions require single-photon energy. If $\hbar\omega < 2E_F$, since the electron states in the conduction band have no vacancy, there will be no interband transition due to the Pauli exclusion principle. Therefore, graphene appears transparent. When $\hbar\omega > 2E_F$, an interband transition will occur by absorbing photons. Therefore, the interband transition state can be turned on or off by voltage modulation of the Fermi level under the fixed incident light [103–105].

The carrier relaxation time of graphene is on the order of picoseconds [101,106], which means that graphene's electro-optical modulation response rate may approach the theoretical value of 500 GHz under certain conditions.

3. Electrically tunable Fermi level

According to the relation $n = C_g(V_g - V_{\text{Dirac}})/e$, the change of gate voltage can modulate the induced charges in the single layer of graphene, where the gate capacitance is C_g, electron charges is e, and the gate voltage corresponding to the charge-neutral Dirac point is V_{Dirac} [107]. And the Fermi energy varies with carrier concentration in $E_F = \hbar V_F \sqrt{\pi n}$ [108]. Here $V_F = 1 \times 10^6$ is the Fermi velocity of Dirac fermions in graphene [109].

The carrier concentration of graphene is changed by gate inducing, rendering it an electronically controlled phase modulator [110].

Compared with the traditional plasmon in three dimensions with metal, the graphene plasmon has relatively low loss in the visible and near-infrared region, but the loss of the plasmon increases with the imaginary part of the dielectric constant of the metal increases in the terahertz band. However, highly doped graphene has relatively low loss and strong field locality in the terahertz band [111]. The properties of graphene plasmons can be modulated by the Fermi level of graphene, the carrier concentration, and the dielectric constant of the medium. So it has a relatively large flexibility [106]. Compared with noble metals, graphene possesses some advantages: high confinement, relatively low loss, and good tunability, which make it a promising plasmonic material.

IV. SP WITH DIFFERENT NANOSTRUCTURES

In addition to choosing different materials, ultrafast devices will also be designed on various nanostructures.

In a broad sense, nanostructure refers to structures whose structural dimensions are in 100 nm in at least one dimension in three-dimensional space or are formed by them as basic building units [103]. It exhibits unique effects different from bulk materials at the subwavelength scale, such as surface effects, quantum size effects, and macroscopic quantum tunneling [112–115], endowing them with excellent physical and chemical properties. Therefore, nanostructures have wide application prospects in many fields like energy utilization, biomedicine, efficient catalysis, protection of environment, and photoelectric detection [116–118].

Among various nanostructures, metal nanostructures have attracted extensive attention because they have special phenomena such as field enhancement, selective absorption, and scattering of light caused by the unique surface plasmon resonance (SPR). Based on their unique size, morphology, and other microstructures with excellent optical, electrical, thermal, magnetic, and mechanical properties, they pay extensive attention to many research fields, such as diagnosis and treatment, environmental protection, and magnetic media [119–122]. Specially, gold, silver, and copper gradually gained a foothold in nanoscience research due to their surface-plasmon properties. Table I summarizes typical nanostructure and different field-enhancement factors based on various nanostructures combining with plasmons. In addition to the independent nanostructures, the perfect wave absorber realized by the thin-film composite layer can also increase the absorption of light, and these composite structures are designed for full absorption from microwaves to the visible [132,133].

In order to apply to different ultrafast devices or to study different physical phenomena such as ultrafast dynamics, kinds of simple metallic nanostructures such as nanotips [123,129], nanowires [78], nanospheres [134], nanorods [71,79,124,125], nanotriangles [71], nanostars [80,126, 127], nanodisks [135,136], composite bowtie and nanorod antennae [9,128,137] have been researched for high density of electron in the apex, which induces a considerable near field.

The highly confined coherent electron wave packets can be generated by ultrafast electron emission based on sharp metallic nanotapers when irradiation of few-cycle laser pulses. The electron wave packets have attosecond duration and strong directivity [38,43,123,130,131,138]. Electron emission is induced by combining the sharp metallic nanotapers and gratings. The structure may serve as an ultrafast electron source for time-resolved low-energy electron microscopy [61,62].

Thanks to nanostructures, the speed of emission electrons is increased. There is a strong field at the taper apex, and the acceleration of electrons happens within the field gradient [131]. The trajectories of photoelectrons generated under strong light-field excitation are largely determined by the magnitude of the quiver amplitude

TABLE I.   Different nanostructures applied to ultrafast field-emission and their key parameters.

| Material	Morphology	Size of the emitting tip	Substrate	Field enhancement (wavelength)	Dominant field enhancement mechanism	The local optical field strength (when accessing strong field emission)
Gold [123]	Nanotip	12 and 22 nm	$\cdots$	7.2 and 5.8 (800 nm)	Plasmon resonance and geometry effect	28 V nm^{-1}
Gold [78]	Nanowire	Diameters between 90 and 190 nm	Tungsten tips	Simulation: 6.6–10.4 (750 nm); Experiment: 5.98 ± 0.24 (750 nm)	Plasmon resonance and geometry effect	$\cdots$
Gold [37]	Nanosphere	Diameter of 90 nm	Si-Au film	1000	Plasmon resonance	50 V nm^{-1}
Gold [79]	Nanorod	150 nm × 50 nm	ZnS	36 (800 nm)	Plasmon resonance	3.5 V nm^{-1}
Gold [124]	Nanorod	70 nm × 20 nm	ITO	60 (795 nm)	Plasmon resonance	3–4.3 V nm^{-1}
Gold [71]	Nanotriangle	Altitude and base: 220, 165 nm	ITO	36 (1058 nm)	Plasmon resonance	540 V nm^{-1}
Gold [125]	Nanorod	95 nm × 180 nm × 40 nm	Nb-doped TiO$_2$	Considering the intensity enhancement factor in the range of 10–1000 (740–800 nm)	localized plasmon resonances	10 GW cm^{-1}
Gold [126]	Nanostars	Tip radii (3.4 nm)	10-nm ITO film	50 (795 nm)	Plasmon resonance and geometry effect	$\cdots$
Gold [127]	Nanostars	5 nm	ITO/SiO$_2$	60 (800 nm)	localized plasmon resonances	$\cdots$
Gold [128]	Bowtie	Each triangle of a bowtie was 75 ± 5 nm in length, had a tip radius of curvature of 18 ± 2 nm, thickness of approximately 18 nm	fused silica	39 (830 nm)	localized plasmon resonances	$\cdots$
Gold [9]	Bowtie	with 90-nm width, 40-nm height, and 260-nm length (20-nm gap)	$\cdots$	Simulation: 50(800 nm)	localized plasmon resonances	0.5 V nm^{-1}
Gold [128]	Bowtie	8-nm gap	fused silica	35	localized plasmon resonances	100 V nm^{-1}
Gold [129]	Nanotip	10 nm	$\cdots$	90 (800 nm)	localized plasmon resonances	$\cdots$
Tungsten [130]	Tip	10–20 nm	$\cdots$	5	geometry effect	/10.4 GV m^{-1}
Gold [131]	Nanotaper	5 nm	$\cdots$	9 (1.65 µm)	localized plasmon resonances	15.4 V nm^{-1}
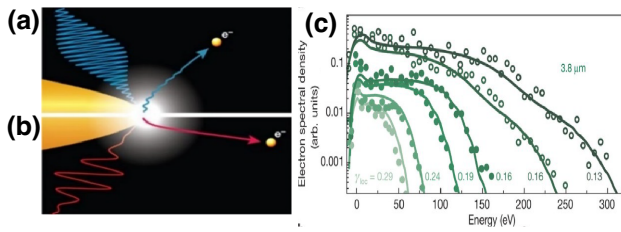
FIG. 13. (a) The trajectories of photoelectrons under the excitation of (a) short wavelength, (b) long wavelength. (c) Kinetic energy spreads of photoelectrons with varying intensities at wavelength 3.8 μm. Experimental (circles) and simulated (solid lines); tip radii of 12 nm (solid circles) and 22 nm (open circles) [123].
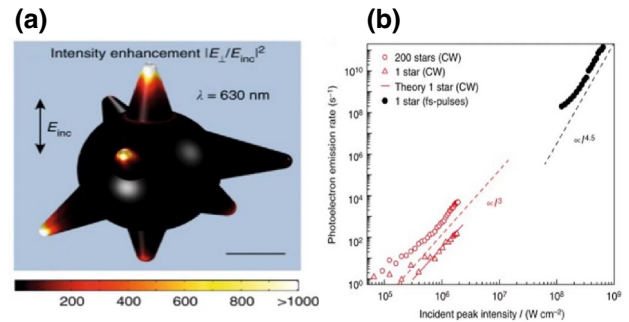

FIG. 14. (a) Simulation of magnitude square of electric field component for a nanostar [an arrow indicates the surface-normal field (20-nm scale bar)]. (b) Light peak intensity for the photoelectron emission rate for single and multiple nanostars [71].

[see Figs. 13(a) and 13(b)], and plasmon-assisted photoinduced emission electrons are accelerated to kinetic energies of hundreds of electronvolts [123] [as displayed in Fig. 13(c)].

The combination of nanostructures and plasmons brings good news for ultrafast devices due to more excellent features and enables better light-matter interactions at not-so-high light intensities. Light-matter interactions controlled by field are fundamental to attosecond science [4,139], expanding from the origin of atomic and molecular science [4,134] to solid [131,140], even the realm of surfaces [56,141], and plasmon nanostructures [9,37,123].

With nanoscale confinement of optical fields and local intensity enhancement, it is easier to access the strong-field regime under the illumination of a few-cycle laser without the intensity of TW cm^{-2}. Benefiting from the huge enhancement, such as 10^3 with nanosphere [37], huge laser intensity exceeding the damage threshold of the sample [142,143] can be voided. Accompanied by significant field enhancements in subwavelength confinement in plasmonic structures, plasmonic gold nanostars reach three-photon photoemission under the excitation of continuous-wave on the order of sub-MW cm^{-2} with exceeding 1000 times of intensity enhancement [80] [as plotted in Fig. 14]. Highly nonlinear phenomena process is observed by continuous wave instead of ubiquitous ultrashort laser pulses in ultrafast nano-optics [144,145].

V. DIFFERENT ULTRAFAST DEVICES BASED ON SP

A. Modulator

Ultrafast devices based on different materials and nanostructures are introduced above, such as the modulator, switch, and microscope electron source. In 1969, Miller proposed the concept of integrated optics [146]. A transmitter, a waveguide, and a receiver form integrated optical interconnects. The integrated optical waveguide is the basic unit of the integrated optical device, which is mainly made of the following materials: lithium niobate, doped silicon dioxide, silicon-silicon-on-insulator, silicon nitride, III–V semiconductor materials, polymers, etc. Although silicon has more than four decades of history as dominated material in solid-state electronics, some other materials with expansion wavelength range and better performance (such as graphene) are used in photonic device alternatives to silicon [147].

The modulator on the optical waveguide mode can impose a data stream. The 3-dB bandwidth of the thin-film lithium niobate modulators was measured as 35 GHz [148]. And the silicon *IQ* modulator reaches 20.1 GHz [149]. Nevertheless, the typical sizes are too large to integrate the dimension on the order of millimeters.

1. Modulator based on metal plasmon

Surface plasmons are utilized to confine light to subwavelength levels meanwhile offer a possibility to enhance light-matter interaction [150], thus enabling the size of devices to be greatly reduced without sacrificing their performance.

Dong-Jin Lee *et al.* proposed a structure of metal-insulator-metal (*M-I-M*) plasmonic waveguide as an electro-optic modulator that modifies the electro-optic in insulator by applying voltage refractive index of polymers in the 2009 International Conference on Photonics in Switching. The power modulation ratios are 3.65 dB, and the modulator length is 2.15 μm [as shown in Fig. 15] [151]. Besides that, high-extinction-ratio (>25 dB), with a total length of 10 μm, ultrafast plasmonic Mach-Zehnder modulator has an electro-optic frequency response larger than 70 GHz [see Fig. 16] [152].

All-metallic Mach-Zehnder modulators were designed for on-chip integration and a simple fabrication process, including the elements—the vertical grating couplers, splitters, polarization rotators, and active section with phase shifters, which can be fabricated on a single metal layer, and an extinction ratio is more than 15 dB [153] [as
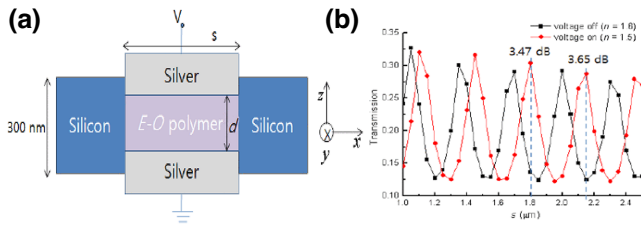
FIG. 15.   (a) Schematic diagram of a *M-I-M* plasmon waveguides for the electro-optic modulator. (b) The voltage-OFF state $n_{\text{eo-polymer}} = 1.6$) (black curve) and the voltage-ON state $n_{\text{eo-polymer}} = 1.5$) (red curve) [151].

depicted in Figs. 17(a) and 17(b)]. There is no speed limitation to the measured frequency response at frequencies up to 70 GHz under the highest signal excitation available for the experiment [as plotted in Fig. 18(b)]. The calculated capacitance of the device itself is 14 fF, and the source impedance is 50 Ω. According to the relationship between the modulator bandwidth and the *RC* constant, the modulation speed of the device exceeds 200 GHz.

The all-metallic modulator works according to the following mechanism.

A multicore fiber couples the signal in or out directly to the metallic grating couplers. *P*-polarized light couples from an optical fiber to surface plasmons and propagates along the upper surface of the metal, as the top surface is the location where surface charges are mainly distributed, last, splits into two beams.

It is necessary to squeeze the surface-plasmon mode into the *M-I-M* waveguide gap plasmon mode for efficient modulating. The conversion from *p*-polarized into *s*-polarized mode can be realized in polarization rotators where the widths of the signal plate w_s and the gap of the waveguide w_g are changed to meet control [153]. Therefore, as w_s and w_g decreases, the charges move from the upper surface to the side. Finally, the model is converted to *s* polarization by increasing w_s [as depicted in Figs. 17(c)–17(e)].

The modulation process is realized in an *M-I-M* waveguide gap that relies on spin coating of a nonlinear optical material that can be fabricated on an insulator surface

FIG. 17.   (a) All-metal devices involving vertical grating coupler (GC), polarization rotator (PR), and Mach-Zehnder interferometer (MZI). (b) Magnified image of a GC with staircase gratings. (c) A *p*-polarized SPP mode on the top surface. (d) Conversion of the two modes in the PR section. (e) *S*-polarized SPP mode [153].

[155]. Surface plasmons are mainly distributed in the upper and lower *M-I-M* waveguides, which are signals awaiting modulation. The modulation module is equivalent to a Mach-Zehnder modulator (MZM). The nonlinear optical material is covered on the upper, and its refractive index will be changed by applying a driving voltage, which will cause the change of the phase of the plasmon in the *M-I-M* waveguide and the intensity of the output signal [as depicted in Fig. 18(a)].

2. Modulator based on graphene plasmon

a. All-optical modulator based on graphene. However, as the performance requirements of photonics technology are improved, researchers have begun to pursue broadband and ultrafast optical modulation. Thence, all-optical modulation in simple configurations with excellent characteristics (low-loss, ultrafast, and broadband optical signal processing) show great potential in applications [154]. Moreover, it is an approach to improve the modulation rate (which is called "electrical bottleneck") and achieve pure
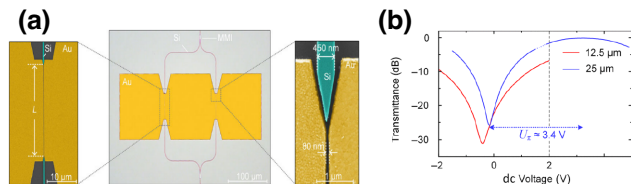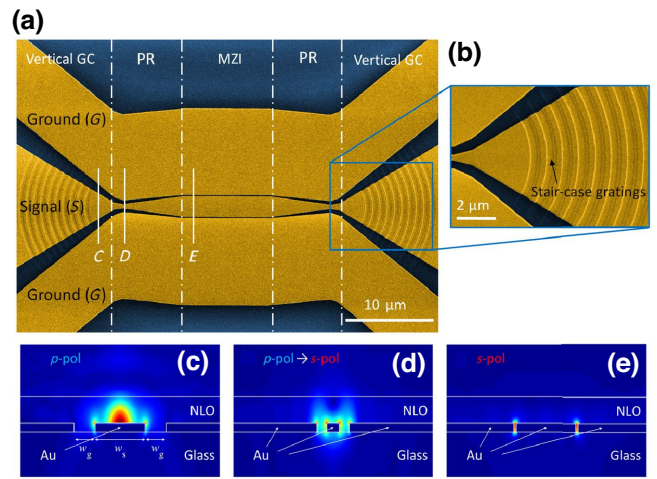

FIG. 16.   (a) The Mach-Zehnder modulator, close-up of plasmonic phase modulators (PPMs) in both arms on the left and close-up of the photonic-plasmonic converter on the right. (b) Normalized power transmission concerning for the applied dc voltage [152].
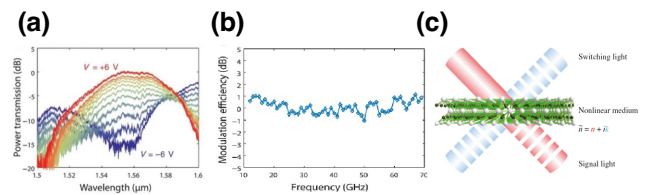

FIG. 18.   (a) The optical power transmission spectrum when switching from −6 to +6 V. (b) The frequency response of the device [153]. (c) Schematic of all-optical modulation [154].

optical communication in the circuit, while the modulation bandwidth is limited to about 1 GHz due to the response of the driving electrical circuit [156].

All-optical modulation is that a switching light beam is used to control a signal light beam [see Fig. 18(c)] [154]. The light-light interaction is achieved by changing the refractive index of the nonlinear medium. The ultrafast optical response can be achieved by combining plasmon with many 2D materials, such as graphene, which have recently attracted much attention [5,157–160]. 2D materials can be directly attached to optical fibers or other waveguides. A fiber with dielectric nanostructures at its facet by electron beam based on lithography makes an efficient collection of light come true [161]. Fiber optics combined with different materials and structures suit all-optical networks with miniature sizes, diverse integrated functions, and low insertion losses [162]. Furthermore, a phase-gradient plasmonic metasurface on the tip of an optical fiber can detect very low concentrations of streptavidin with very high sensitivity [163].

Graphene-based all-optical modulators have been studied for several years [5,157]. The reason why the intensity and phase of the light going through the graphene-clad microfiber (GCM) can be modulated is that nonlinear absorption and the Kerr effect of graphene [164] [see Fig. 19(a)]. The switching light modulates the output signal, and the relaxation of the excited carriers limits the response time of the modulator. According to the report, the relaxation time of photogenerated carriers in graphene is extremely short (10 fs to several picoseconds) [165].

The modulation process of the GCM modulator can be described as follows. Two kinds of wave are coupled into the GCM: a weak infrared signal light and a switching light. The former will experience significant attenuation because of absorption in graphene [164]. When the latter is turned on, interband transitions of charge carriers in graphene are excited, which results in lower attenuation of the signal wave as the frequency of light absorption of graphene shifting to higher frequency. Therefore, the signal light is modulated [as shown in Fig. 19(b)].

Though the operating speed of the GCM optical modulator is 2.2 ps (equivalent to a modulation rate of 200 GHz) and a maximal modulation depth is 38%, the device needs a power density on the order of GW cm^{-2} and the diameter of microfiber is 1.2 μm [as plotted in Figs. 19(c) and 19(d)] [5]. We must find an approach to achieve low energy, smaller modulators.

b. All-optical modulator based on graphene plasmon. Silicon is employed in most modulators in silicon photonics (SiPh) [166]. Furthermore, all-optical modulation can be achieved based on the nonlinear effects [167]. However, it is not conducive to low-energy consumption and miniaturization for silicon's low inherent nonlinear Kerr effects: 10^{-18} m^2 W^{-1}. However, for the silicon platform is economical, we can integrate it with high Kerr-coefficient materials to keep the advantage. For example, graphene, where the Kerr coefficient is from 10^{-7} to 10^{-13} m^2 W^{-1}, can be integrated into a silicon waveguide [168] to design a graphene-on-silicon (GOS) all-optical modulator. Therefore, the Kerr refractive index can be modulated to control the nonlinear response when an optical pump shines on the graphene. The relationship between the refractive index and the optical conductivity of graphene can be derived from the formula:

$$n = \sqrt{1 + \frac{i\sigma}{\epsilon_0 \omega d_{\text{eff}}}}, \qquad (6)$$

where d_{eff} represents the graphene's layer thickness, which is approximated to 0.3 nm in Ref. [5].

Gold (Au) stripes are placed on graphene based on the principle of GOS modulation to obtain a modulator with a faster response time and lower-energy consumption. This structure can motivate plasmon, which will boost optical absorption effectively originating from the enhancement of its interaction with light [158–160].

The design of an all-optical modulator based on a GOS waveguide has been studied, which performs at incident intensities of MW cm^{-2}, and it is in sub-mm device lengths [158] [as plotted in Fig. 20]. The slot waveguide obtains the best size through simulation optimization, which makes SPPs highly confined in the slits with the significant interaction of light graphene. Based on a graphene-plasmonic slot waveguide (GPSW), an all-optical modulator obtains a modulation efficiency of 0.21 dB μm^{-1} with
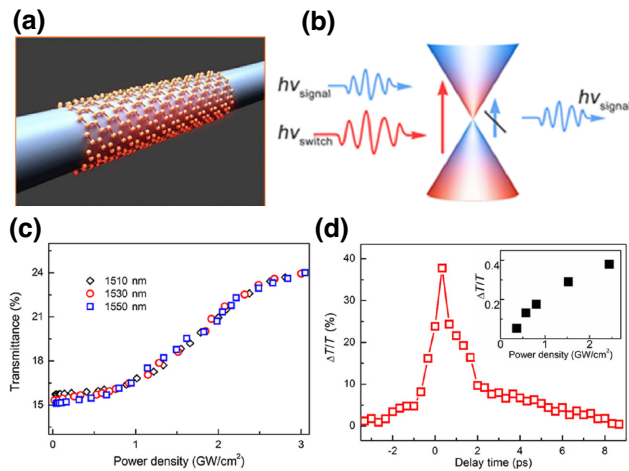

FIG. 19. (a) Schematic illustration of a graphene-clad microfiber modulator. (b) The diagrammatic sketch shows pump and probe carriers in the band structure of graphene [164]. (c) The transmittance of the GCM varies by peak power of 220-fs pulses. (d) Differential transmittance of the probe light changes by the pump-probe time delay where the pump power is 200 nW. The inset describes the modulation depth as a function of the pump intensity [5].
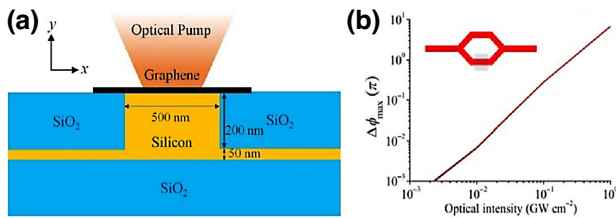
FIG. 20. (a) Schematic cross section of an all-optical modulator based on graphene on silicon. (b) Maximum phase shift of the modulator versus optical pump intensity [158].

average optical intensity on the order of W cm^{-2} [as shown in Fig. 21] [159].

Recently, research in this area has further developed. These researches make us closer to future on-chip interconnection. Theoretically, the proposed graphene all-optical modulator based on plasmon-enhanced reaches a bandwidth beyond 100 GHz and reaches ultrafast (<120 fs) and energy-efficient (<0.6 pJ) switching [160]. By simulating, 12-μm-long modulator reveals a high extinction ratio (ER) of 3.5 dB, and the modulation efficiency is around 0.28 dB μm^{-1} [see Fig. 22]. Moreover, it is characterized by a 6.2-dB insertion loss (IL), given by IL $= 10 \log_{10} (1/T_{\mathrm{on}})$ (T_{on} represents the transmission capacity of the probe signal when introducing the pump signal), which is the lowest IL in recent reports of such modulators.

B. Switch

1. Switch-based plasmon

Photonic integrated circuit (PIC) is an alternative integrated chip structure that uses photons as information carriers [146]. Photonic chips are expected to break through current integrated circuits' inherent electronic bottleneck limitations and achieve greater bandwidth and higher processing speed.

Ultrafast optical switches are fundamental elements in optical communication systems and integrated optical logic circuits [169,170]. Compared with optical-electric-optical conversion, opto-optical switch can steer optical signals directly in an integrated photonic chip and actively
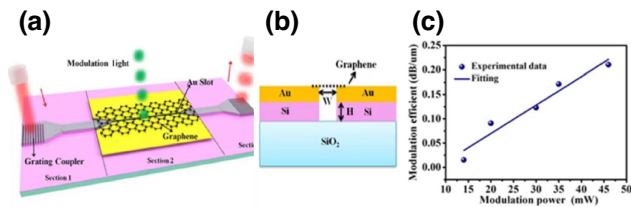

FIG. 21. (a) Schematic of the all-optical modulator based on GPSW. (b) Cross section of the designed structure. (c) Changes in the modulation efficiency in dependence of modulation power for the signal light at 1550 nm [159].
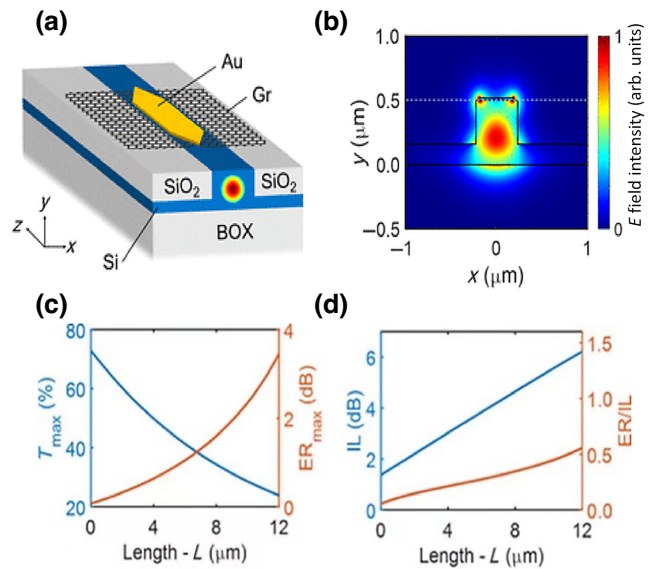

FIG. 22. (a) Illustration of the designed all-optical modulator. (b) Electric field diagram of the propagating mode in the device. (c) Maximum transmitted power ($T_{\max}$) and the maximum ER (ER$_{\max}$) versus the length of the modulator (L). (d) IL and ER:IL ratio versus the modulator length (L). $\lambda = 1550$ nm [160].

control the transmission of light, avoiding time delays and overcoming the speed limitation of electric switches [171].

The all-optical switch is the photonic communication device that use only the interaction between photons and media to alter the refractive index or absorption coefficient of medium, therefore the "ON" and "OFF" effects can be achieved by changing the transmittance of light [146].

Research has demonstrated ultrafast switching with less than 1 ps [172,173]. However, a large driving energy of microjoules to nanojoules per pulse is required. The switching energy of a few hundred femtojoules was estimated, but the switching time is 150 ps in an all-optical switch based on an InP/(In, As)P nanowires are focused for all-optical switching in Ref. [174]. This is attributed to the fast and very strong optical nonlinearity, such as the Kerr effect, depending on the refractive index changed by the intensity of the light [171]. However, they require large driving energy to achieve that speed due to the intrinsically small optical nonlinearity. The general problem is to trade off speed and energy. As the low nonlinear interaction efficiency can be overcome by an intensive light field, the trade-off can be broken by taking advantage of the strong light confinement [171]. It is necessary to confine light locally, maintaining the switching energy small while ensuring high light fields and local energy densities.

There is an approach that creating a graphene-loaded plasmonic nanowaveguide with nonlinear absorption can break that barrier [171,175], which harnesses the strong light confinement and very large, flat broadband absorption and fast carrier relaxation dynamics of graphene
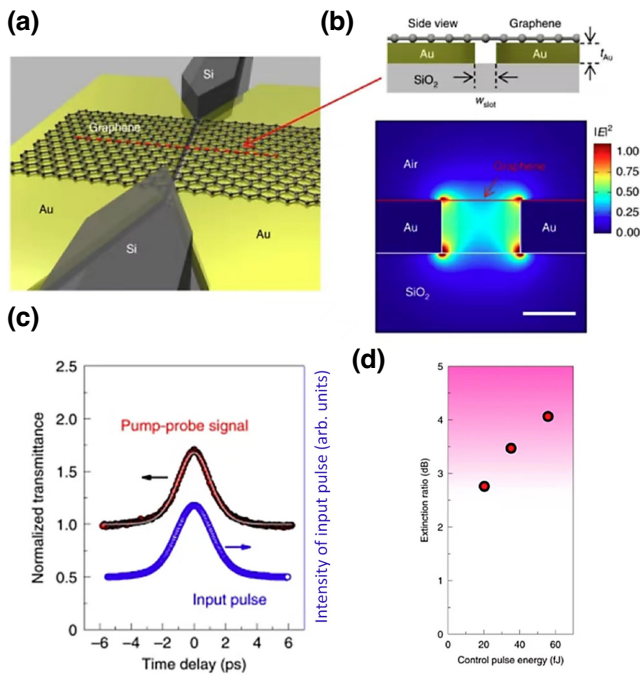
FIG. 23. (a) Schematic of the *M-I-M*–WG based on graphene. (b) Cross section of the structure at the broken red line. (c) Simulation of the structure's magnitude square of field profile ($|E|^2$). Here $\lambda = 1550$ nm and scale bar of 20 nm. (d) All-optical switching with the pump-probe method in the device. (e) The energy of control pulse versus the extinction ratio for the device [175].

[176]. Now, Ono, together with colleagues, reported a *M-I-M* waveguide based on graphene in nature photonics, which demonstrates the smallest switching energy for opto-optical switches with subpicosecond: driving energy of only 35 fJ as well as switching time of only 260 fs while the extinction ratio is 3.5 dB in this case [175] [see Fig. 23].

2. Switch based on plasmon-assisted electron emission

In recent years, another possibility for implementing switches has emerged. Foratid *et al.* proposed a semiconductor-free microelectronic device independent of carriers within semiconductors excited by laser intensities of about 1 W cm^{-2} with a low bias voltage (<10 V) [44]. The combination of ac field (photoemission assisted by LSPRs) and static field injects electrons into gas or vacuum, and the magnitude of emission current is 100 nA without laser while over 40 μA with laser [as depicted in Fig. 4]. The magnitude of the current is controlled by the laser as shown in the paper. The designed device can perform as an optical switch by turning ON and OFF states with a switch ratio of 4000. The electron emission time can be roughly estimated. The resonance wavelength is 785 nm. The photoemission time is around subpicosecond within half an optical period according to the semiclassical three-step model [139].

There are also some researches on how to connect and disconnect the circuit by controlling the emission current state with light [47,48]. They propose a structure that can access electron emission from a metal surface into a nanogap vacuum. Mostly metallic resonant surfaces can incite surface plasmon with enhanced and confined electric fields, which can significantly reduce excitation power. And those structures combine electrical and optical excitations of electrons. Moreover, this method achieves ultrafast electron emission utilizing ultrafast laser on the nanometer scale. This might be used as ultrafast photoswitches and beneficial for on-chip devices.

C. Microscope electron source
1. Microscope from 2D and 3D to 4D

Electrons are not only the basic particles that make up matter but are also a useful tool for humans to observe the microscopic world. With the help of the short wavelength of electrons, it is theoretically possible to achieve ultrafast microscopic imaging with temporal and spatial resolution as low as angstroms and attosecond scales. British physicist Thomson discovered electrons in 1897 [177] and French physicist De Broglie proposed the material wave hypothesis in 1923, and then in 1927, physicist Thomson discovered the diffraction phenomenon of electrons in experiments [178], which proved the wave-particle duality of electrons, and opened up the use of electron probes for materials, chemistry, and biological sciences. The electron microscope can be regarded as the most beneficial tool for spatial imaging of structures [179].

Since the invention of the transmission electron microscope in the 1930s [177], it has provided picometer-level wavelengths beyond the "minutes" of Hooke's Micrographia in the 17th century. The possibility of imaging atoms in real space with a resolution bellow 0.1 nm has come true. Although, 2D and 3D microscopies enable the imaging with subnanometer and even ångstrom-scale spatial resolution, they are static structures. Therefore, the fourth-dimension time must be introduced considering some transformations, including complex transient structures or studying dynamic process. As the extension of the fourth dimension, time, the motion can be visualized. A temporal reference point can be established by launching a femtosecond pulse on the sample. The pulse can be called the clocking or pump pulse. Changes that occur in the motion can be described after the establishment of time zero [180]. On the other hand, attosecond transient absorption spectroscopy (ATAS) in graphene provides a way to imaging techniques [181].

The application of time-dependent transmission electron microscopy spans areas of research like physical chemistry [182,183], biophysics [184], nanophotonics [185], condensed-matter physics [186], and materials science [187,188], with the ns to fs resolution domain [189,190].

Different from a conventional TEM without femtosecond time resolution, high-time resolution electron microscopes possess at most one electron in each electron pulse, which makes ultrashort pulses of electrons detect the specimen [179].

2. Ultrafast electron microscopy

Femtosecond ultrafast electron microscopy (UEM) based on traditional TEM is one of the key ways for time-resolved electron microscopy [179,191]. The conception of "single-electron" imaging is the foundation of ultrafast electron microscopy (UEM) [191]. Unlike the conventional microscopes with a random spread of electron [180], in UEM, each electron is independent and does not interfere with each other, and the electron packets have femtosecond precision [as shown in Fig. 24, left]. Despite the fact that timed single-electron packets are used in UEM, images can be obtained as well as conventional microscopes using many electrons.

The ultrafast electron microscope (UEM) is shown in Ref. [156] or Ref. [155], where the interface to the femtosecond optical system can be extended to feed a laser system [as plotted in Fig. 24, right]. Part of the beam can generate the electron pulse train, which is one electron per pulse. After a well-defined delay time, the other optical beam illuminates the specimen and heats or excites it simultaneously, thus defining the zero of time.

3. Ultrafast point-projection electron microscopy (UPEM)

Projection imaging is a method of UEM where the ratio of detector-tip-distance (D) to sample-tip-distance (d)
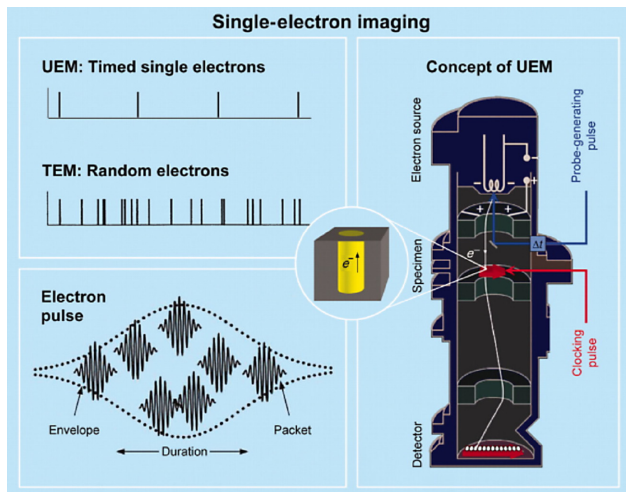

FIG. 24. (a) Conceptual diagram of single-electron imaging and UEM. Schematics of single-electron packets and random electrons used in imaging (upper left). The electron-pulse envelope and individual electron packets (lower left). Schematic of concept of UEM (right) [180].
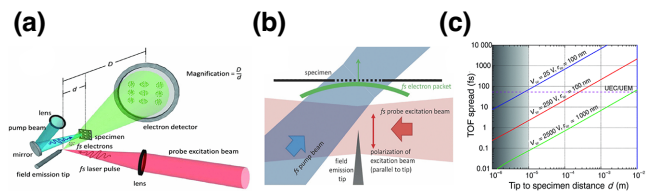

FIG. 25. (a) Diagrammatic sketch of the femtosecond photoelectron point projection microscope. (b) Enlarged view of the tip and specimen area. The blue and red pulse's concentrating diameter is 10 μm. (c) Temporal distribution in time-of-flight versus tip-to-specimen distance with various acceleration voltages [193].

defines the magnification in the image, and high-resolution microscopic information is not affected by aberrations without electron lenses [192] [as shown in Fig. 25(a)].

Some imaging for plasmas and photoelectrons with ultrafast electron imaging technology has been demonstrated with picosecond and femtosecond temporal resolution but with hundred μm level of spatial resolution [194–196].

Quinonez *et al.* reported a femtosecond photoelectron point projection microscope (fsPPM) by introducing laser-triggered metal nanotaper emitters based on electron point projection microscope techniques [193]. During imaging, the electron emission process occurs within approximately 100 fs [as displayed in Fig. 25(c)], showing higher temporal resolution compared with traditional UEM. The microscope demonstrates that the nanowires become visible with a diameter of approximately 100 nm. With the help of the near-field enhancement at nanostructures, the spatial resolution of time-resolved microscopy can be improved [46,145]. Therefore, metallic nanotips with local field enhancement have been another nanoscale electron source in UEM [38,43,123,197,198].

The technology of combining point projection microscopes with ultrafast field emission tip sources has been reported [193,199]. With optimized field emitters, a spatial resolution of point projection microscopy (PPM) has achieved a few nm in recent years [192,200,201]. How to find an approach to increase the temporal and spatial resolution simultaneously is the problem to be solved.

a. Plasmon-driven UPEM. The focal spot size formed by the laser irradiation will limit the minimum distance of the emitter sample, which influences the temporal and spatial resolution in PPM [197]. If the spot covers the emitter and the specimen, a femtosecond laser pulse as excitation may irradiate on the specimen, followed by another femtosecond laser pulse which generates the femtosecond electron pulse to image simultaneously. [The probe excitation pulse (red) and the pump pulse (blue) may concentrate on the tip at the same time] [see Fig. 25(b)]. This results in undesired sample heating or photoemission for coinstantaneous sample illumination. To prevent those from
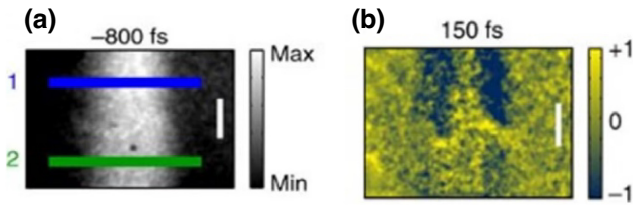
FIG. 26. (a) Projection image of the same InP nanowires recorded at a negative time delay. (b) Normalized difference plot after optical excitation [199].

happening, which restrict both the spatial (approximately 100 nm) [62,193,199] together with temporal resolution (approximately 100 fs) [199,202] of PPM (Fig. 26), it is necessary to limit the emitter-sample distance to at least a few (tens of) microns.

To maintain the resolution and avoid the direct illumination of the apex like some time-resolved point-projection microscopes [193,199,202], a method that the electron emission from the nanotip with no direct laser-driven apex should be considered. How to focus optical radiance on the nanoscale and avoid just a little part of the concentrated excitation energy can be solved by coupling tapered optical fibers or single-walled carbon nanotubes [203,204]. Therefore, plasmon (regarded as an evanescent wave, which can replace direct vertex lighting) may offer the elegant solution [197,205] where plasma waves generated by light shining far away from the apex of the taper emitter.

The grating coupling can confine the photon energy locally by combining the grating with the sharp cone. And as the geometric radius of the cone shrinks, the energy is finally concentrated at the vertex. A nanometer-scale broadband light source has been realized [43] [as plotted in Fig. 27], showing better energy concentrating in the second position. Some wedge [206–208] and cone [13,58,209,210] structures have been used to achieve plasmon focusing at the apex of these structures to generate femtosecond electronic wave packets. The ultrashort electron pulses have been generated by nanofocusing femtosecond SPPs [13,61,62,72,197] [see Fig. 28(d)]. And the SPP is induced by femtosecond laser irradiating on a sharp gold nanotaper. There are some researches about surface plasmon-driven UEM as follows.

Vogelsang *et al.* realized a compact alternative electron source by using focused gallium ion-beam lithography to engrave seven parallel slit gratings with a width of 800 nm and a depth of 400 nm at a distance of 40–50 μm from the apex of the gold cone, and they have implemented its application in point-projection microscopy [197]. The focal spot 30 μm² of incident laser is compressed into 500 nm² of nanofocus. Hence, the energy at the nanofocusing is 250 fJ while the pulse energy is 160 pJ, demonstrating that electron emission is incited at exceedingly low energies. The electrons excited by light irradiating on the grating are
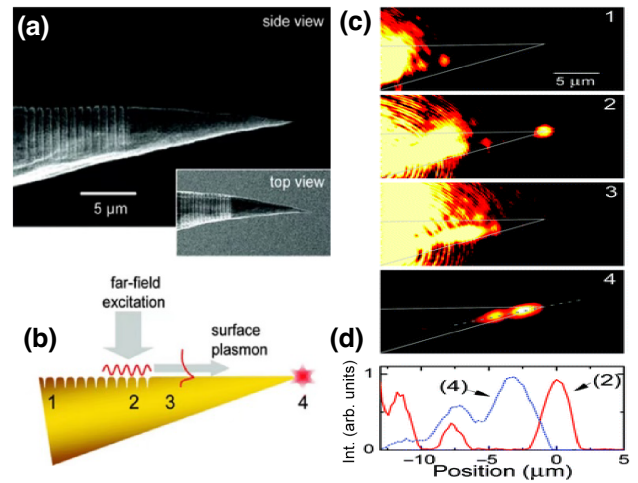

FIG. 27. (a) SEM image of the nanofabricated metallic tips with gratings. (b) SPPs on the grating propagating toward the tip apex. (c) The scattered light images for four irradiation positions are indicated in (b). The curves in (d) displays sections through images 2 and 4 corresponding to the dashed line in image 4 [205].

50 times higher than the electrons excited by light directly shining the apex [as plotted in Figs. 28(a)–28(c)].

Müller *et al.* imaged a single InP nanowire (NW) by employing the nanofocusing plasmon-triggered nanotips. They assessed the temporal resolution in fsPPM by using SPP-triggered electron source by mapping three different electron energy distributions. According to the energy distribution of the electrons, the electron pulse duration keeps sub-10 fs within a distance of 1–3 μm from the nanotip to sample [62] [as displayed in Fig. 29].

Vogelsang *et al.* generated SPPs by laser pulses with a duration of 15 fs at a distance of 80 μm from the nanocone
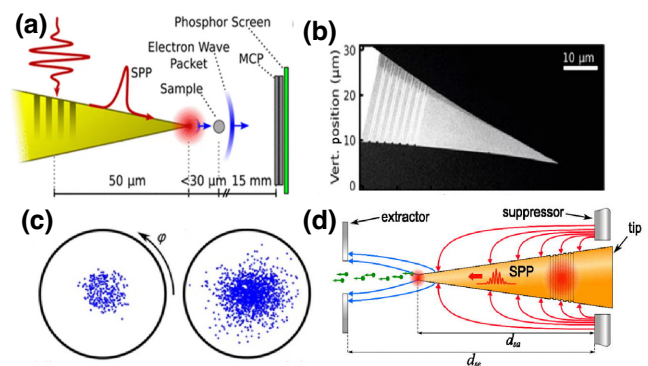
FIG. 28. (a) Schematic diagram of electron emission device incited by laser pulses. A microchannel detects emission electrons from a sharp taper. (b) SEM image of a sample. (c) Electron distribution on the MCP phosphor screen for emission by dc excitation (left) and by laser illumination (right) [197]. (d) For certain voltages, the electron emission is only from the taper apex not the grating coupler. Integration of tip and an electron gun assembly enable applications in ultrafast electron imaging [61,62].

FIG. 29. (a) Schematic illustration of fsPPM for imaging an individual InP nanowire. (b) Simulation of electron pulse duration τ_{el} at the sample in regard to the distance of tip and sample with different initial energy distributions σ_E [62].

apex. The SPPs concentrate to a size of 15 nm at taper apex to generate ultrashort electron probe pulses [72] [as displayed in Fig. 30(a)]. The deflection of probe pulses is achieved by a cloud of electrons incited from the gap of a nanoresonator generated by a pum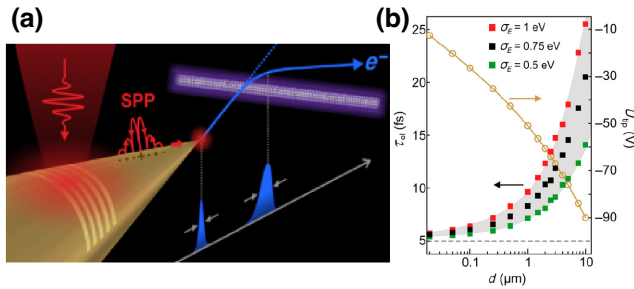p laser shining. The nanoresonator is a piece of polycrystalline gold film 30 nm thin, which is dug out two 400-nm-diameter holes, and a 30-nm-wide channel connects the two holes [see Fig. 30(b)].

The interaction between probing electrons and nanoantenna excited by light changes the transient UPEM image. Transmission of the probe electrons is blocked by electrons generated by pump light exciting nanoantennas [211–213]. Those interaction shows a dynamic scene of how the electron cloud evolves in time and space as the change of the time delay between the pump light and probe pulse [see Fig. 30(c)]. The UPEM provides a spatial resolution and
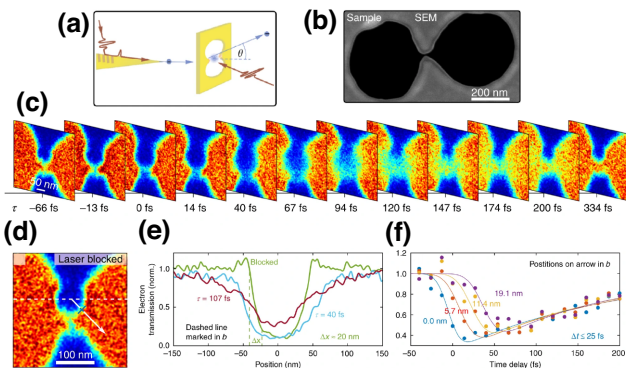

FIG. 30. (a) UPEM imaging of photoemission enhanced by plasmon. (b) SEM image of the device. (c) Shadow image of the central gap region with different time delays. (d) The UPEM image of the sample without optical excitation. (e) Electron transmission concerning different delay times along the dashed white line shown in (b). (f) Electron transmission drops from 90% to 10% in 25 fs. The four curves are points taken equidistantly along the white arrows in *b* [72].

temporal resolution of 20 nm and 25 fs, respectively [72] [as depicted Fig. 30(e) and 30(f)].

VI. CONCLUSION AND OUTLOOK

Ultrafast devices based on nanomaterials or nanostructures are emerging as a topic of interest because they meet the demand for fast, even ultrafast. Where ultrafast electron emission expands our comprehension of ultrafast electron dynamics. With the aid of plasmons, highly localized electromagnetic fields can be realized at lower energies to control the trajectories of electrons on nanometer spatial scales and the variation on subcycle temporal.

The researches present awareness and knowledge of the interaction between light and nanoscale matters through plasmons with a wide variety of structures. And the light required for electron emission from high power density lasers to low power, from ultrashort laser pulses to continuous wave where the materials that excite plasmons ranging from 3D metals to 2D graphene have resulted in broadband plasmons suitable for diverse devices to achieve faster, lower-energy consumption, and smaller size.

Applying graphene to a silicon-based integrated modulator can not only make use of the advantages of silicon-based integrated devices but also achieve performance breakthroughs, including wideband, low-cost, and integration. However, the all-optical modulator based on graphene plasmon proposed by Ono *et al.* may have been difficult to break through in a graphene-saturated absorption modulator (achieving an extinction ratio of 3.5 dB with a pumping energy of 35 fJ and whose switching speed reaches 260 fs). Some methods can achieve breakthroughs in speed and energy consumption in the future, considering using other two-dimensional materials besides graphene, such as black phosphorus, or optimizing the modulator structure and patterning two-dimensional materials.

The advantages of silicon-based integrated circuits can be applied to integrated optics. In addition to graphene mentioned in this paper, the polymers with an excellent nonlinear response (huge nonlinear coefficient and femtosecond response time) can be studied and combined with silicon-based metasurface to realize all-optical switches with better performance. Conversely, a switch based on plasmon-assisted electron emission is not limited by carrier recombination time. However, this kind of switch is rare in an application.

With people's exploration of nature, the demand for microscopes is increasing. Time-resolved emission electron microscope requires high laser power and photon energy because imaging is based on photoelectric emission. In order to pursue femtosecond time resolution and nanoscale or even higher spatial resolution, an ultrafast electron microscope (four-dimensional electron microscope) appears. Future research should consider the trends

from 4D UEM to 5D UEM (adding such as energy resolution) and even attosecond electron microscopy.

———————

[1] Alexander Ziegler, Ultrafast materials science and 4D imaging with atomic resolution both in space and time, MRS Bull. **36,** 121 (2011).

[2] P. B. Corkum and Ferenc Krausz, Attosecond science, Nat. Phys. **3,** 381 (2007).

[3] Giuseppe Sansone, Luca Poletto, and Mauro Nisoli, High-energy attosecond light sources, Nat. Photonics **5,** 655 (2011).

[4] Ferenc Krausz and Misha Ivanov, Attosecond physics, Rev. Mod. Phys. **81,** 163 (2009).

[5] Wei Li, Bigeng Chen, Chao Meng, Wei Fang, Yao Xiao, Xiyuan Li, Zhifang Hu, Yingxin Xu, Limin Tong, Hongqing Wang, Weitao Liu, Jiming Bao, and Y. Ron Shen, Ultrafast all-optical graphene modulator, Nano Lett. **14,** 955 (2014).

[6] L. Sandrin, S. Catheline, M. Tanter, X. Hennequin, and M. Fink, Time-resolved pulsed elastography with ultrafast ultrasonic imaging, Ultrason. Imaging **21,** 259 (1999).

[7] Shenghan Zhou, Ke Chen, Matthew Thomas Cole, Zhenjun Li, Jun Chen, Chi Li, and Qing Dai, Ultrafast field-emission electron sources based on nanomaterials, Adv. Mater. **31,** 1805845 (2019).

[8] B. Barwick, C. Corder, J. Strohaber, N. Chandler-Smith, C. Uiterwaal, and H. Batelaan, Laser-induced ultrafast electron emission from a field emission tip, New J. Phys. **9,** 142 (2007).

[9] Péter Dombi, Anton Hörl, Péter Rácz, István Márton, Andreas Trügler, Joachim R. Krenn, and Ulrich Hohenester, Ultrafast strong-field photoemission from plasmonic nanoparticles, Nano. Lett. **13,** 674 (2013).

[10] Vilson R. Almeida, Carlos A. Barrios, Roberto R. Panepucci, and Michal Lipson, All-optical control of light on a silicon chip, Nature **431,** 1081 (2004).

[11] Viktoriia E. Babicheva, Alexandra Boltasseva, and Andrei V. Lavrinenko, Transparent conducting oxides for electro-optical plasmonic modulators, Nanophotonics **4,** 165 (2015).

[12] Thomas Søndergaard and Sergey I. Bozhevolnyi, Metal nano-strip optical resonators, Opt. Express **15,** 4198 (2007).

[13] Mark I. Stockman, Nanofocusing of Optical Energy in Tapered Plasmonic Waveguides, Phys. Rev. Lett. **93,** 137404 (2004).

[14] Rui-Qi Li, D. Hernángomez-Pérez, F. J. García-Vidal, and A. I. Fernández-Domínguez, Transformation Optics Approach to Plasmon-Exciton Strong Coupling in Nanocavities, Phys. Rev. Lett. **117,** 107401 (2016).

[15] H. Ditlbacher, J. R. Krenn, A. Hohenau, A. Leitner, and F. R. Aussenegg, Efficiency of local light-plasmon coupling, Appl. Phys. Lett. **83,** 3665 (2003).

[16] P. Törmä and W. L. Barnes, Strong coupling between surface plasmon polaritons and emitters: A review, Rep. Progr. Phys. **78,** 013901 (2014).

[17] Jakub Dostálek, Hana Vaisocherová, and J. Homola, Multichannel surface plasmon resonance biosensor with wavelength division multiplexing, Sens. Actuators, B **108,** 758 (2005).

[18] Matthew J. Lockyear, Alastair P. Hibbins, J. Roy Sambles, and Christopher R. Lawrence, Surface-topography-induced enhanced transmission and directivity of microwave radiation through a subwavelength circular metal aperture, Appl. Phys. Lett. **84,** 2040 (2004).

[19] Afshin Partovi, David Peale, Matthias Wuttig, Cherry A. Murray, George Zydzik, Leslie Hopkins, Kirk Baldwin, William S. Hobson, James Wynn, and John Lopata, *et al.*, High-power laser light source for near-field optics and its application to high-density optical data storage, Appl. Phys. Lett. **75,** 1515 (1999).

[20] L. Cao and Mark L. Brongersma, Ultrafast developments, Nat. Photonics **3,** 12 (2009).

[21] Dmitri K. Gramotnev and Sergey I. Bozhevolnyi, Plasmonics beyond the diffraction limit, Nat. Photonics **4,** 83 (2010).

[22] Jian Wei You, Qian Ma, Zhihao Lan, Qiang Xiao, Nicolae C. Panoiu, and Tie Jun Cui, Reprogrammable plasmonic topological insulators with ultrafast control, Nat. Commun. **12,** 5468 (2021).

[23] Heinz Raether, Surface plasmons on gratings (2006), p. 91.

[24] Kevin F. MacDonald, Zsolt L. Sámson, Mark I. Stockman, and Nikolay I. Zheludev, Ultrafast active plasmonics, Nat. Photonics **3,** 55 (2009).

[25] Thomas Nikolajsen, Kristjan Leosson, and Sergey I. Bozhevolnyi, Surface plasmon polariton based modulators and switches operating at telecom wavelengths, Appl. Phys. Lett. **85,** 5833 (2004).

[26] Domenico Pacifici, Henri J. Lezec, and Harry A. Atwater, All-optical modulation by plasmonic excitation of CdSe quantum dots, Nat. Photonics **1,** 402 (2007).

[27] Yichen Ye, Yiyuan Xie, Yuzhu Liu, Shujian Wang, Jingping Zhang, and Yong Liu, Design of a compact logic device based on plasmon-induced transparency, IEEE Photonics Technol. Lett. **29,** 647 (2017).

[28] Kunhua Wen, Yihua Hu, Li Chen, Jinyun Zhou, Miao He, Liang Lei, and Ziming Meng, Plasmonic-induced absorption and transparency based on a compact ring-groove joint MIM waveguide structure, IEEE Photonics J. **8,** 1 (2016).

[29] Hiromi Okamoto and Kohei Imura, Near-field optical imaging of enhanced electric fields and plasmon waves in metal nanostructures, Prog. Surf. Sci. **84,** 199 (2009).

[30] Jeffrey N. Anker, W. Paige Hall, Olga Lyandres, Nilam C. Shah, Jing Zhao, and Richard P. Van Duyne, Biosensing with plasmonic nanosensors, Nat. Mater. **7,** 442 (2008).

[31] Qiaoliang Bao and Kian Ping Loh, Graphene photonics, plasmonics, and broadband optoelectronic devices, ACS Nano **6,** 3677 (2012).

[32] Vivian E. Ferry, Luke A. Sweatlock, Domenico Pacifici, and Harry A. Atwater, Plasmonic nanostructure design for efficient light coupling into solar cells, Nano Lett. **8,** 4391 (2008).

[33] Marek Procházka, Surface-enhanced Raman spectroscopy (2016), p. 1.

[34] P. Dombi, S. E. Irvine, P. Rácz, M. Lenner, N. Kroó, G. Farkas, A. Mitrofanov, A. Baltuška, T. Fuji, F. Krausz, and A. Y. Elezzabi, Observation of few-cycle, strong-field phenomena in surface plasmon fields, Opt. Express **18,** 24206 (2010).

[35] Nicolò Maccaferri, Sophie Meuret, Nikolay Kornienko, and Deep Jariwala, Speeding up nanoscience and nanotechnology with ultrafast plasmonics, Nano Lett. **20,** 5593 (2020).

[36] Peng Cun, Meng Wang, Cuiying Huang, Pei Huang, Xinkui He, Zhiyi Wei, and Xinping Zhang, Conductive connection induced speed-up of localized-surface-plasmon dynamics, J. Opt. **20,** 014011 (2017).

[37] Florian Schertz, Marcus Schmelzeisen, Maximilian Kreiter, Hans-Joachim Elmers, and Gerd Schönhense, Field Emission of Electrons Generated by the Near Field of Strongly Coupled Plasmons, Phys. Rev. Lett. **108,** 237602 (2012).

[38] Peter Hommelhoff, Yvan Sortais, Anoush Aghajani-Talesh, and Mark A. Kasevich, Field Emission Tip as a Nanometer Source of Free Electron Femtosecond Pulses, Phys. Rev. Lett. **96,** 077401 (2006).

[39] Hirofumi Yanagisawa, Christian Hafner, Patrick Doná, Martin Klöckner, Dominik Leuenberger, Thomas Greber, Matthias Hengsberger, and Jürg Osterwalder, Optical Control of Field-Emission Sites by Femtosecond Laser Pulses, Phys. Rev. Lett. **103,** 257603 (2009).

[40] C. I. Blaga, F. Catoire, P. Colosimo, G. G. Paulus, H. G. Muller, P. Agostini, and L. F. DiMauro, Strong-field photoionization revisited, Nat. Phys. **5,** 335 (2009).

[41] R. Bormann, M. Gulde, A. Weismann, S. V. Yalunin, and C. Ropers, Tip-Enhanced Strong-Field Photoemission, Phys. Rev. Lett. **105,** 147601 (2010).

[42] L. V. Keldysh, Ionization in the field of a strong electromagnetic wave, Sov. Phys. JETP **20,** 1307 (1965).

[43] C. Ropers, D. R. Solli, C. P. Schulz, C. Lienau, and T. Elsaesser, Localized Multiphoton Emission of Femtosecond Electron Pulses from Metal Nanotips, Phys. Rev. Lett. **98,** 043907 (2007).

[44] Ebrahim Forati, Tyler J. Dill, Andrea R. Tao, and Dan Sievenpiper, Photoemission-based microelectronic devices, Nat. Commun. **7,** 13399 (2016).

[45] Yves C. Martin, Hendrik F. Hamann, and H. Kumar Wickramasinghe, Strength of the electric field in apertureless near-field optical microscopy, J. Appl. Phys. **89,** 5774 (2001).

[46] P. Rácz, S. M. Teichmann, M. F. Ciappina, J. A. Pérez-Hernández, A. Thai, J. Fekete, A. Y. Elezzabi, L. Veisz, J. Biegert, and P. Dombi, in *2015 11th Conference on Lasers and Electro-Optics Pacific Rim (CLEO-PR)* (IEEE, 2015), Vol. 3, p. 1.

[47] Shiva Piltan and Dan Sievenpiper, Field enhancement in plasmonic nanostructures, J. Opt. **20,** 055401 (2018).

[48] Philipp Zimmermann, Alexander Hötger, Noelia Fernandez, Anna Nolinder, Kai Müller, Jonathan J. Finley, and Alexander W. Holleitner, Toward plasmonic tunnel gaps for nanoscale photoemission currents by on-chip laser ablation, Nano Lett. **19,** 1172 (2019).

[49] William L. Barnes, Alain Dereux, and Thomas W. Ebbesen, Surface plasmon subwavelength optics, Nature **424,** 824 (2003).

[50] Jacob B. Khurgin, How to deal with the loss in plasmonics and metamaterials, Nat. Nanotechnol. **10,** 2 (2015).

[51] E. Kretschmann and H. Raether, Notizen: Radiative decay of non radiative surface plasmons excited by light, Z. Naturforsch. A **23,** 2135 (1968).

[52] A. P. Hibbins, E. Hendry, M. J. Lockyear, and J. R. Sambles, Prism coupling to 'designer' surface plasmons, Opt. Express **16,** 20441 (2008).

[53] Osamu Takayama, A. A. Bogdanov, and Andrei V. Lavrinenko, Photonic surface waves on metamaterial interfaces, J. Phys.: Condens. Matter **29,** 463001 (2017).

[54] Jiří Homola, Surface plasmon resonance sensors for detection of chemical and biological species, Chem. Rev. **108,** 462 (2008).

[55] Barbora Špačková, Piotr Wrobel, and Markéta Bocková, Optical biosensors based on plasmonic nanostructures: a review, Proc. IEEE **104,** 2380 (2016).

[56] P. Rácz, S. E. Irvine, M. Lenner, A. Mitrofanov, A. Baltuška, A. Y. Elezzabi, and P. Dombi, Strong-field plasmonic electron acceleration with few-cycle, phase-stabilized laser pulses, Appl. Phys. Lett. **98,** 111116 (2011).

[57] F. Keilmann, Surface-polariton propagation for scanning near-field optical microscopy application, J. Microsc. **194,** 567 (1999).

[58] A. J. Babadjanyan, N. L. Margaryan, and Kh V. Nerkararyan, Superfocusing of surface polaritons in the conical structure, J. Appl. Phys. **87,** 3785 (2000).

[59] Catalin C. Neacsu, Samuel Berweger, Robert L. Olmon, Laxmikant V. Saraf, Claus Ropers, and Markus B. Raschke, Near-field localization in plasmonic superfocusing: A nanoemitter on a tip, Nano Lett. **10,** 592 (2010).

[60] Samuel Berweger, Joanna M. Atkin, Xiaoji G. Xu, Robert L. Olmon, and Markus B. Raschke, Femtosecond nanofocusing with full optical waveform control, Nano Lett. **11,** 4309 (2011).

[61] Gero Storeck, Simon Vogelgesang, Murat Sivis, Sascha Schäfer, and Claus Ropers, Nanotip-based photoelectron microgun for ultrafast leed, Struct. Dyn. **4,** 044024 (2017).

[62] Melanie Müller, Vasily Kravtsov, Alexander Paarmann, Markus B. Raschke, and Ralph Ernstorfer, Nanofocused plasmon-driven sub-10 fs electron point source, ACS Photonics **3,** 611 (2016).

[63] P. B. Johnson and R. W. Christy, Optical constants of the noble metals, Phys. Rev. B **6,** 4370 (1972).

[64] J. P. Marton and B. D. Jordan, Optical properties of aggregated metal systems: Interband transitions, Phys. Rev. B **15,** 1719 (1977).

[65] M. A. Noginov, G. Zhu, M. Bahoura, J. Adegoke, C. E. Small, B. A. Ritzo, V. P. Drachev, and V. M. Shalaev, Enhancement of surface plasmons in an Ag aggregate by optical gain in a dielectric medium, Opt. Lett. **31,** 3022 (2006).

[66] P. R. West, S. Ishii, G. V. Naik, N. K. Emani, V. M. Shalaev, and A. Boltasseva, Searching for better plasmonic materials, Laser. Photonics Rev. **4,** 795 (2010).

[67] Gururaj V. Naik, Vladimir M. Shalaev, and Alexandra Boltasseva, Alternative plasmonic materials: Beyond gold and silver, Adv. Mater. **25,** 3264 (2013).

[68] Joseph M. Luther, Prashant K. Jain, Trevor Ewers, and A. Paul Alivisatos, Localized surface plasmon resonances

arising from free carriers in doped quantum dots, Nat. Mater. **10**, 361 (2011).

[69] Vilius Palenskis, The effective density of randomly moving electrons and related characteristics of materials with degenerate electron gas, AIP Adv. **4**, 047119 (2014).

[70] Cecilia Noguez, Surface plasmons on metal nanoparticles: The influence of shape and physical environment, J. Phys. Chem. C **111**, 3806 (2007).

[71] William P. Putnam, Richard G. Hobbs, Phillip D. Keathley, Karl K. Berggren, and Franz X. Kärtner, Optical-field-controlled photoemission from plasmonic nanoparticles, Nat. Phys. **13**, 335 (2017).

[72] Jan Vogelsang, Germann Hergert, Dong Wang, Petra Groß, and Christoph Lienau, Observing charge separation in nanoantennas via ultrafast point-projection electron microscopy, Light: Sci. Appl. **7**, 55 (2018).

[73] Rahul Raveendran Nair, Peter Blake, Alexander N. Grigorenko, Konstantin S. Novoselov, Tim J. Booth, Tobias Stauber, Nuno M. R. Peres, and Andre K. Geim, Fine structure constant defines visual transparency of graphene, Science **320**, 1308 (2008).

[74] Hugen Yan, Fengnian Xia, Wenjuan Zhu, Marcus Freitag, Christos Dimitrakopoulos, Ageeth A. Bol, George Tulevski, and Phaedon Avouris, Infrared spectroscopy of wafer-scale graphene, ACS Nano **5**, 9854 (2011).

[75] Francisco J. Garcia-Vidal, Antonio I. Fernández-Domínguez, Luis Martin-Moreno, Hao Chi Zhang, Wenxuan Tang, Ruwen Peng, and Tie Jun Cui, Spoof surface plasmon photonics, Rev. Mod. Phys. **94**, 025004 (2022).

[76] Prashant K. Jain, Kyeong Seok Lee, Ivan H. El-Sayed, and Mostafa A. El-Sayed, Calculated absorption and scattering properties of gold nanoparticles of different size, shape, and composition: Applications in biological imaging and biomedicine, J. Phys. Chem. B **110**, 7238 (2006).

[77] Benjamin J. Wiley, Sang Hyuk Im, Zhi-Yuan Li, Joeseph McLellan, Andrew Siekkinen, and Younan Xia, Maneuvering the surface plasmon resonance of silver nanostructures through shape-controlled synthesis, J. Phys. Chem. B **110**, 15666 (2006).

[78] B. Ahn, Johannes Schötz, Mijeong Kang, W. A. Okell, S. Mitra, Benjamin Förg, Sergey Zherebtsov, Frederik Süßmann, Christian Burger, and Matthias Kübel, *et al.*, Attosecond-controlled photoemission from metal nanowire tips in the few-electron regime, APL Photonics **2**, 036104 (2017).

[79] F. Kusa, K. E. Echternkamp, Georg Herink, Claus Ropers, and S. Ashihara, Optical field emission from resonant gold nanorods driven by femtosecond mid-infrared pulses, AIP Adv. **5**, 077138 (2015).

[80] Murat Sivis, Nicolas Pazos-Perez, Renwen Yu, Ramon Alvarez-Puebla, F. Javier García de Abajo, and Claus Ropers, Continuous-wave multiphoton photoemission from plasmonic nanostars, Commun. Phys. **1**, 13 (2018).

[81] K. S. Novoselov, S. V. Morozov, T. M. G. Mohinddin, L. A. Ponomarenko, D. C. Elias, R. Yang, I. I. Barbolina, P. Blake, T. J. Booth, D. Jiang, J. Giesbers, E. W. Hill, and A. K. Geim, Electronic properties of graphene, Phys. Status Solidi (b) **244**, 4106 (2007).

[82] A. N. Grigorenko, M. Polini, and K. S. Novoselov, Graphene plasmonics, Nat. Photonics **6**, 749 (2012).

[83] F. Karimi, A. H. Davoody, and I. Knezevic, Dielectric function and plasmons in graphene: A self-consistent-field calculation within a Markovian master equation formalism, Phys. Rev. B **93**, 205421 (2016).

[84] E. H. Hwang and S. Das Sarma, Dielectric function, screening, and plasmons in two-dimensional graphene, Phys. Rev. B **75**, 205418 (2007).

[85] S. A. Mikhailov and K. Ziegler, New Electromagnetic Mode in Graphene, Phys. Rev. Lett. **99**, 016803 (2007).

[86] Jianing Chen, Michela Badioli, Pablo Alonso-González, Sukosin Thongrattanasiri, Florian Huth, Johann Osmond, Marko Spasenović, Alba Centeno, Amaia Pesquera, Philippe Godignon, Amaia Zurutuza Elorza, Nicolas Camara, F. Javier García de Abajo, Rainer Hillenbrand, and Frank H. L. Koppens, Optical nano-imaging of gate-tunable graphene plasmons, Nature **487**, 77 (2012).

[87] Siyuan Luo, Yanan Wang, Xin Tong, and Zhiming Wang, Graphene-based optical modulators, Nanoscale Res. Lett. **10**, 199 (2015).

[88] Christopher T. Phare, Yoon-Ho Daniel Lee, Jaime Cardenas, and Michal Lipson, Graphene electro-optic modulator with 30 GHz bandwidth, Nat. Photonics **9**, 511 (2015).

[89] Qiushi Guo, Cheng Li, Bingchen Deng, Shaofan Yuan, Francisco Guinea, and Fengnian Xia, Infrared nanophotonics based on graphene plasmonics, ACS Photonics **4**, 2989 (2017).

[90] García de Abajo and F. Javier, Graphene plasmonics: Challenges and opportunities, ACS Photonics **1**, 135 (2014).

[91] Jian Wei You, Zhihao Lan, and Nicolae C. Panoiu, Four-wave mixing of topological edge plasmons in graphene metasurfaces, Sci. Adv. **6**, eaaz3910 (2020).

[92] Guichuan Xing, Hongchen Guo, Xinhai Zhang, Tze Chien Sum, Cheng Sum, and Hon Alfred Huan, The physics of ultrafast saturable absorption in graphene, Opt. Express **18**, 4564 (2010).

[93] Daniel B. S. Soh, Ryan Hamerly, and Hideo Mabuchi, Comprehensive analysis of the optical Kerr coefficient of graphene, Phys. Rev. A **94**, 023845 (2016).

[94] Daniel Popa, Zicai Sun, Tawfique Hasan, Felice Torrisi, Fengqiu Wang, and Andrea Carlo Ferrari, Graphene Q-switched, tunable fiber laser, Appl. Phys. Lett. **98**, 073106 (2011).

[95] Ferda Canbaz, Nurbek Kakenov, Coskun Kocabas, Umıt Demırbas, and Alphan Sennaroglu, Generation of sub-20-fs pulses from a graphene mode-locked laser, Opt. Express **25**, 2834 (2017).

[96] Kin Fai Mak, Matthew Y. Sfeir, Yang Wu, Chun Hung Lui, James A. Misewich, and Tony F. Heinz, Measurement of the Optical Conductivity of Graphene, Phys. Rev. Lett. **101**, 196405 (2008).

[97] A. B. Kuzmenko, E. van Heumen, F. Carbone, and D. van der Marel, Universal Optical Conductance of Graphite, Phys. Rev. Lett. **100**, 117401 (2008).

[98] Claire M. Watts, Xianliang Liu, and Willie J. Padilla, Metamaterial electromagnetic wave absorbers (adv. mater. 23/2012), Adv. Mater. **24**, OP181-OP181 (2012).

[99] Yurui Qu, Qiang Li, Hanmo Gong, Kaikai Du, Songang Bai, Ding Zhao, Hui Ye, and Min Qiu, Spatially and spectrally resolved narrowband optical absorber based on 2D

grating nanostructures on metallic films, Adv. Opt. Mater. **4,** 480 (2016).

[100] Chu-Cai Guo, Zhi-Hong Zhu, Xiao-Dong Yuan, Wei-Min Ye, Ken Liu, Jian-Fa Zhang, Wei Xu, and Shi-Qiao Qin, Experimental demonstration of total absorption over 99% in the near infrared for monolayer-graphene-based sub-wavelength structures, Adv. Opt. Mater. **4,** 1955 (2016).

[101] S. Winnerl, M. Orlita, P. Plochocka, P. Kossacki, M. Potemski, T. Winzer, E. Malic, A. Knorr, M. Sprinkle, C. Berger, W. A. de Heer, H. Schneider, and M. Helm, Carrier Relaxation in Epitaxial Graphene Photoexcited Near the Dirac Point, Phys. Rev. Lett. **107,** 237401 (2011).

[102] Edward D. Palik, *Handbook of Optical Constants of Solids* (Academic press, 1998), Vol. 3.

[103] H. Gleiter, Nanostructured materials: Basic concepts and microstructure, Acta Mater. **48,** 1 (2000).

[104] Feng Wang, Yuanbo Zhang, Chuanshan Tian, Caglar Girit, Alex Zettl, Michael Crommie, and Y. Ron Shen, Gate-variable optical transitions in graphene, Science **320,** 206 (2008).

[105] Z. Q. Li, E. A. Henriksen, Z. Jiang, Z. Hao, M. C. Martin, P. Kim, H. L. Stormer, and D. N. Basov, Dirac charge dynamics in graphene by infrared spectroscopy, Nat. Phys. **4,** 532 (2008).

[106] Tobias Kampfrath, Luca Perfetti, Florian Schapper, Christian Frischkorn, and Martin Wolf, Strongly Coupled Optical Phonons in the Ultrafast Dynamics of the Electronic Energy and Current Relaxation in Graphite, Phys. Rev. Lett. **95,** 187403 (2005).

[107] Jun Yan, Yuanbo Zhang, Philip Kim, and Aron Pinczuk, Electric Field Effect Tuning of Electron-Phonon Coupling in Graphene, Phys. Rev. Lett. **98,** 166802 (2007).

[108] Jia-Ming Liu and I-Tan Lin, *Graphene Photonics* (Cambridge University Press, 2018).

[109] Lei Ren, Qi Zhang, Jun Yao, Zhengzong Sun, Ryosuke Kaneko, Zheng Yan, Sébastien Nanot, Zhong Jin, Iwao Kawayama, Masayoshi Tonouchi, James M. Tour, and Junichiro Kono, Terahertz and infrared spectroscopy of gated large-area graphene, Nano Lett. **12,** 3711 (2012).

[110] Jacek Gosciniak and Dawn T. H. Tan, Theoretical investigation of graphene-based photonic modulators, Sci. Rep. **3,** 1897 (2013).

[111] Xiaoguang Luo, Teng Qiu, Weibing Lu, and Zhenhua Ni, Plasmons in graphene: Recent progress and applications, Mater. Sci. Eng. R: Rep. **74,** 351 (2013).

[112] Stefan Auer and Daan Frenkel, Suppression of crystal nucleation in polydisperse colloids due to increase of the surface free energy, Nature **413,** 711 (2001).

[113] Philip Ball and Laura Garwin, Science at the atomic scale, Nature **355,** 761 (1992).

[114] Bernard Barbara and Wolfgang Wernsdorfer, Quantum tunneling effect in magnetic particles, Curr. Opin. Solid State Mater. Sci. **2,** 220 (1997).

[115] Prashant V. Kamat, Photochemistry on nonreactive and reactive (semiconductor) surfaces, Chem. Rev. **93,** 267 (1993).

[116] Yu-Liang Chen, Chi-Young Lee, and Hsin-Tien Chiu, Growth of gold nanowires on flexible substrate for highly sensitive biosensing: Detection of thrombin as an example, J. Mater. Chem. B **1,** 186 (2013).

[117] Qipeng Lu, Zhenda Lu, Yunzhang Lu, Longfeng Lv, Yu Ning, Hongxia Yu, Yanbing Hou, and Yadong Yin, Photocatalytic synthesis and photovoltaic application of Ag-Tio$_2$ nanorod composites, Nano Lett. **13,** 5698 (2013).

[118] Younan Xia, Weiyang Li, Claire M. Cobley, Jingyi Chen, Xiaohu Xia, Qiang Zhang, Miaoxin Yang, Eun Chul Cho, and Paige K. Brown, Gold nanocages: From synthesis to theranostic applications, Acc. Chem. Res. **44,** 914 (2011).

[119] Harry A. Atwater and Albert Polman, Plasmonics for improved photovoltaic devices, Nat. Mater. **9,** 205 (2010).

[120] Zygmunt Gryczynski, Joanna Lukomska, Joseph R. Lakowicz, Evgenia G. Matveeva, and Ignacy Gryczynski, Depolarized light scattering from silver nanoparticles, Chem. Phys. Lett. **421,** 189 (2006).

[121] Suchita A. Kalele, Neha R. Tiwari, Suresh Gosavi, and Sulabha K. Kulkarni, Plasmon-assisted photonics at the nanoscale, J. Nanophotonics **1,** 012501 (2007).

[122] Kyeong-Seok Lee and Mostafa A. El-Sayed, Gold and silver nanoparticles in sensing and imaging: Sensitivity of plasmon response to size, shape, and metal composition, J. Phys. Chem. B **110,** 19220 (2006).

[123] G. Herink, D. R. Solli, M. Gulde, and C. Ropers, Field-driven photoemission from nanostructures quenches the quiver motion, Nature **483,** 190 (2012).

[124] Martin Lehr, Benjamin Foerster, Mathias Schmitt, Katja Krüger, Carsten Sönnichsen, Gerd Schönhense, and Hans-Joachim Elmers, Momentum distribution of electrons emitted from resonantly excited individual gold nanorods, Nano Lett. **17,** 6606 (2017).

[125] Quan Sun, Kosei Ueno, Han Yu, Atsushi Kubo, Yasutaka Matsuo, and Hiroaki Misawa, Direct imaging of the near field and dynamics of surface plasmon resonance on gold nanostructures using photoemission electron microscopy, Light: Sci. Appl. **2,** e118 (2013).

[126] Jacob Pettine, Priscilla Choo, Fabio Medeghini, Teri W. Odom, and David J. Nesbitt, Plasmonic nanostar photocathodes for optically-controlled directional currents, Nat. Commun. **11,** 1367 (2020).

[127] Calin Hrelescu, Tapan K. Sau, Andrey L. Rogach, Frank Jäckel, Guillaume Laurent, Ludovic Douillard, and Fabrice Charra, Selective excitation of individual plasmonic hotspots at the tips of single gold nanostars, Nano Lett. **11,** 402 (2011).

[128] Tobias Rybka, Markus Ludwig, Michael F. Schmalz, Vanessa Knittel, Daniele Brida, and Alfred Leitenstorfer, Sub-cycle optical phase control of nanotunnelling in the single-electron regime, Nat. Photonics **10,** 667 (2016).

[129] L. Wimmer, G. Herink, D. R. Solli, S. V. Yalunin, K. E. Echternkamp, and C. Ropers, Terahertz control of nanotip photoemission, Nat. Phys. **10,** 432 (2014).

[130] Michael Krüger, Markus Schenk, and Peter Hommelhoff, Attosecond control of electrons emitted from a nanoscale metal tip, Nature **475,** 78 (2011).

[131] Doo Jae Park, Bjoern Piglosiewicz, Slawa Schmidt, Heiko Kollmann, Manfred Mascheck, and Christoph Lienau, Strong Field Acceleration and Steering of Ultrafast Electron Pulses from a Sharp Metallic Nanotip, Phys. Rev. Lett. **109,** 244803 (2012).

[132] Y. Ra'di, C. R. Simovski, and S. A. Tretyakov, Thin Perfect Absorbers for Electromagnetic Waves: Theory,

Design, and Realizations, Phys. Rev. Appl. **3,** 037001 (2015).

[133] Rasoul Alaee, Mohammad Albooyeh, and Carsten Rockstuhl, Theory of metasurface based perfect absorbers, J. Phys. D: Appl. Phys. **50,** 503002 (2017).

[134] G. Sansone, E. Benedetti, F. Calegari, C. Vozzi, L. Avaldi, R. Flammini, L. Poletto, P. Villoresi, C. Altucci, R. Velotta, S. Stagira, S. De Silvestri, and M. Nisoli, Isolated single-cycle attosecond pulses, Science **314,** 443 (2006).

[135] Anton Samusev, Ivan Mukhin, Radu Malureanu, Osamu Takayama, Dmitry V. Permyakov, Ivan S. Sinev, Dmitry Baranov, Oleh Yermakov, Ivan V. Iorsh, Andrey A. Bogdanov, and Andrei V. Lavrinenko, Polarization-resolved characterization of plasmon waves supported by an anisotropic metasurface, Opt. Express **25,** 32631 (2017).

[136] O. V. Kotov and Yu. E. Lozovik, Enhanced optical activity in hyperbolic metasurfaces, Phys. Rev. B **96,** 235403 (2017).

[137] P. J. Schuck, D. P. Fromm, A. Sundaramurthy, G. S. Kino, and W. E. Moerner, Improving the Mismatch Between Light and Nanoscale Objects with Gold Bowtie Nanoantennas, Phys. Rev. Lett. **94,** 017402 (2005).

[138] Peter Hommelhoff, Catherine Kealhofer, and Mark A. Kasevich, Ultrafast Electron Pulses from a Tungsten Tip Triggered by Low-Power Femtosecond Laser Pulses, Phys. Rev. Lett. **97,** 247402 (2006).

[139] P. B. Corkum, Plasma Perspective on Strong Field Multiphoton Ionization, Phys. Rev. Lett. **71,** 1994 (1993).

[140] Phillip D. Keathley, Alexander Sell, William P. Putnam, Stephen Guerrera, Luis Velásquez-García, and Franz X. Kärtner, Strong-field photoemission from silicon field emitter arrays, Ann. Phys. **525,** 144 (2013).

[141] S. E. Irvine, A. Dechant, and A. Y. Elezzabi, Generation of 0.4-keV Femtosecond Electron Pulses using Impulsively Excited Surface Plasmons, Phys. Rev. Lett. **93,** 184801 (2004).

[142] J. P. Girardeau-Montaut and C. Girardeau-Montaut, Theory of ultrashort nonlinear multiphoton photoelectric emission from metals, Phys. Rev. B **51,** 13560 (1995).

[143] S. A. Hilbert, A. Neukirch, C. J. G. J. Uiterwaal, and H. Batelaan, Exploring temporal and rate limits of laser-induced electron emission, J. Phys. B: At., Mol. Opt. Phys., **42,** 141001 (2009).

[144] Kuiru Li, Mark I. Stockman, and David J. Bergman, Self-Similar Chain of Metal Nanospheres as an Efficient Nanolens, Phys. Rev. Lett. **91,** 227402 (2003).

[145] Martin Aeschlimann, Michael Bauer, Daniela Bayer, Tobias Brixner, F. Javier García de Abajo, Walter Pfeiffer, Martin Rohmer, Christian Spindler, and Felix Steeb, Adaptive subwavelength control of nano-optical fields, Nature **446,** 301 (2007).

[146] Stewart E. Miller, Integrated optics: An introduction, Bell Syst. Tech. J. **48,** 2059 (1969).

[147] Thomas Mueller, Fengnian Xia, and Phaedon Avouris, Graphene photodetectors for high-speed optical communications, Nat. Photonics **4,** 297 (2010).

[148] Hao Xu, Xianyao Li, Xi Xiao, Peiji Zhou, Zhiyong Li, Jinzhong Yu, and Yude Yu, High-speed silicon modulator with band equalization, Opt. Lett. **39,** 4839 (2014).

[149] Jiachuan Lin, Hassan Sepehrian, Leslie A. Rusch, and Wei Shi, in *Optical Fiber Communication Conference* (Optica Publishing Group, 2018), p. Tu2E.4.

[150] Huakang Yu, Yusi Peng, Yong Yang, and Zhi-Yuan Li, Plasmon-enhanced light–matter interactions and applications, npj Comput. Mater. **5,** 45 (2019).

[151] Dong-Jin Lee, Jun-Ho Sung, Seung-Gol Lee, Se-Geun Park, El-Hang Lee, and O. Beom-Hoan, in *2009 International Conference on Photonics in Switching*, (Pisa, Italy, 2009), p. 1.

[152] W. Heni, C. Haffner, B. Baeuerle, Y. Fedoryshyn, A. Josten, D. Hillerkuss, J. Niegemann, A. Melikyan, M. Kohl, D. L. Elder, L. R. Dalton, C. Hafner, and J. Leuthold, 108 Gbit/s plasmonic Mach–Zehnder modulator with >70-GHz electrical bandwidth, J. Lightwave Technol. **34,** 393 (2016).

[153] Masafumi Ayata, Yuriy Fedoryshyn, Wolfgang Heni, Benedikt Baeuerle, Arne Josten, Marco Zahner, Ueli Koch, Yannick Salamin, Claudia Hoessbacher, Christian Haffner, Delwin L. Elder, Larry R. Dalton, and Juerg Leuthold, High-speed plasmonic modulator in a single metal layer, Science **358,** 630 (2017).

[154] Haitao Chen, Cong Wang, Hao Ouyang, Yufeng Song, and Tian Jiang, All-optical modulation with 2D layered materials: Status and prospects, Nanophotonics **9,** 2107 (2020).

[155] Delwin L. Elder, Christian Haffner, Wolfgang Heni, Yuriy Fedoryshyn, Kerry E. Garrett, Lewis E. Johnson, Rachael A. Campbell, Jose D. Avila, Bruce H. Robinson, Juerg Leuthold, and Larry R. Dalton, Effect of rigid bridge-protection units, quadrupolar interactions, and blending in organic electro-optic chromophores, Chem. Mater. **29,** 6457 (2017).

[156] Andrew Alduino and Mario Paniccia, Wiring electronics with light, Nat. Photonics **1,** 153 (2007).

[157] Shaoliang Yu, Xiaoqin Wu, Keren Chen, Bigeng Chen, Xin Guo, Daoxin Dai, Limin Tong, Weitao Liu, and Y. Ron Shen, All-optical graphene modulator based on optical Kerr phase shift, Optica **3,** 541 (2016).

[158] Kelvin J. A. Ooi, Peng Chuen Leong, Lay Kee Ang, and Dawn T. H. Tan, All-optical control on a graphene-on-silicon waveguide modulator, Sci. Rep. **7,** 12748 (2017).

[159] Feiying Sun, Liangping Xia, Changbin Nie, Ciyuan Qiu, Linlong Tang, Jun Shen, Tai Sun, Leyong Yu, Peng Wu, Shaoyun Yin, Shihan Yan, and Chunlei Du, An all-optical modulator based on a graphene-plasmonic slot waveguide at 1550 nm, Appl. Phys. Express **12,** 042009 (2019).

[160] Mohammed AlAloul and Mahmoud Rasras, Low insertion loss plasmon-enhanced graphene all-optical modulator, ACS Omega **6,** 7576 (2021).

[161] Oleh Yermakov, Henrik Schneidewind, Uwe Hübner, Torsten Wieduwilt, Matthias Zeisberger, Andrey Bogdanov, Yuri Kivshar, and Markus A. Schmidt, Nanostructure-empowered efficient coupling of light into optical fibers at extraordinarily large angles, ACS Photonics **7,** 2834 (2020).

[162] Yifeng Xiong and Fei Xu, Multifunctional integration on optical fiber tips: Challenges and opportunities, Adv. Photonics **2,** 064001 (2020).

[163] Marco Consales, Giuseppe Quero, Sara Spaziani, Maria Principe, Alberto Micco, Vincenzo Galdi, Antonello Cutolo, and Andrea Cusano, Metasurface-enhanced lab-on-fiber biosensors, Laser Photonics Rev. **14,** 2000180 (2020).

[164] Han Zhang, Stéphane Virally, Qiaoliang Bao, Loh Kian Ping, Serge Massar, Nicolas Godbout, and Pascal Kockaert, Z-scan measurement of the nonlinear refractive index of graphene, Opt. Lett. **37,** 1856 (2012).

[165] Jahan M. Dawlaty, Shriram Shivaraman, Mvs Chandrashekhar, Farhan Rana, and Michael G. Spencer, Measurement of ultrafast carrier dynamics in epitaxial graphene, Appl. Phys. Lett. **92,** 042116 (2008).

[166] Deji Akinwande, Cedric Huyghebaert, Ching-Hua Wang, Martha I. Serna, Stijn Goossens, Lain-Jong Li, H.-S. Philip Wong, and Frank H. L. Koppens, Graphene and two-dimensional materials for silicon technology, Nature **573,** 507 (2019).

[167] H. John Caulfield and Shlomi Dolev, Why future supercomputing requires optics, Nat. Photonics **4,** 261 (2010).

[168] E. Hendry, P. J. Hale, J. Moger, A. K. Savchenko, and S. A. Mikhailov, Coherent Nonlinear Optical Response of Graphene, Phys. Rev. Lett. **105,** 097401 (2010).

[169] T. Hira, T. Homma, T. Uchiyama, K. Kuwamura, Y. Kihara, and T. Saiki, All-optical switching of localized surface plasmon resonance in single gold nanosandwich using GeSbTe film as an active medium, Appl. Phys. Lett. **106,** 031105 (2015).

[170] Peijun Guo, Richard D. Schaller, John B. Ketterson, and Robert P. H. Chang, Ultrafast switching of tunable infrared plasmons in indium tin oxide nanorod arrays with large absolute amplitude, Nat. Photonics **10,** 267 (2016).

[171] Thomas Purdy, Bright squeezed light reduces back-action, Nat. Photonics **14,** 1 (2020).

[172] Ye Liu, Fei Qin, Zhi-Yi Wei, Qing-Bo Meng, Dao-Zhong Zhang, and Zhi-Yuan Li, 10 fs ultrafast all-optical switching in polystyrene nonlinear photonic crystals, Appl. Phys. Lett. **95,** 131116 (2009).

[173] Mengxin Ren, Baohua Jia, Jun-Yu Ou, Eric Plum, Jianfa Zhang, Kevin F. MacDonald, Andrey E. Nikolaenko, Jingjun Xu, Min Gu, and Nikolay I. Zheludev, Nanostructured plasmonic medium for terahertz bandwidth all-optical switching, Adv. Mater. **23,** 5540 (2011).

[174] Masato Takiguchi, Naotomo Takemura, Kouta Tateno, Kengo Nozaki, Satoshi Sasaki, Sylvain Sergent, Eiichi. Kuramochi, Tabijah Wasawo, Atsushi Yokoo, Akihiko Shinya, and Masaya Notomi, All-optical InAsP/InP nanowire switches integrated in a Si photonic crystal, ACS Photonics **7,** 1016 (2020).

[175] Masaaki Ono, Masanori Hata, Masato Tsunekawa, Kengo Nozaki, Hisashi Sumikura, Hisashi Chiba, and Masaya Notomi, Ultrafast and energy-efficient all-optical switching with graphene-loaded deep-subwavelength plasmonic waveguides, Nat. Photonics **14,** 37 (2020).

[176] K. S. Novoselov, A. K. Geim, S. V. Morozov, D. Jiang, M. I. Katsnelson, I. V. Grigorieva, S. V. Dubonos, and A. A. Firsov, Two-dimensional gas of massless Dirac fermions in graphene, Nature **438,** 197 (2005).

[177] Joseph John Thomson, Xl. cathode rays, London Edinburgh Dublin Philos. Mag. J. Sci. **44,** 293 (1897).

[178] G. P. Thomson and A. Reid, Diffraction of cathode rays by a thin film, Nature **119,** 890 (1927).

[179] Vladimir A. Lobastov, Ramesh Srinivasan, and Ahmed H. Zewail, Four-dimensional ultrafast electron microscopy, Proc. Natl. Acad. Sci. **102,** 7069 (2005).

[180] Ahmed H. Zewail, Four-dimensional electron microscopy, Science **328,** 187 (2010).

[181] Giovanni Cistaro, Luis Plaja, Fernando Martín, and Antonio Picón, Attosecond x-ray transient absorption spectroscopy in graphene, Phys. Rev. Res. **3,** 013144 (2021).

[182] Fabrizio Carbone, Oh-Hoon Kwon, and Ahmed H. Zewail, Dynamics of chemical bonding mapped by energy-resolved 4D electron microscopy, Science **325,** 181 (2009).

[183] Fabrizio Carbone, Brett Barwick, Oh-Hoon Kwon, Hyun Soon Park, J. Spencer Baskin, and Ahmed H. Zewail, Eels femtosecond resolved in 4D ultrafast electron microscopy, Chem. Phys. Lett. **468,** 107 (2009).

[184] David J. Flannigan, Brett Barwick, and Ahmed H. Zewail, Biological imaging with 4d ultrafast electron microscopy, Proc. Natl. Acad. Sci. **107,** 9933 (2010).

[185] Brett Barwick, David J. Flannigan, and Ahmed H. Zewail, Photon-induced near-field electron microscopy, Nature **462,** 902 (2009).

[186] Brett Barwick, Hyun Soon Park, Oh-Hoon Kwon, J. Spencer Baskin, and Ahmed H. Zewail, 4D imaging of transient structures and morphologies in ultrafast electron microscopy, Science **322,** 1227 (2008).

[187] Judy S. Kim, Thomas LaGrange, Bryan W. Reed, Mitra L. Taheri, Michael R. Armstrong, Wayne E. King, Nigel D. Browning, and Geoffrey H. Campbell, Imaging of transient structures using nanosecond in situ TEM, Science **321,** 1472 (2008).

[188] P. Musumeci, J. T. Moody, C. M. Scoby, M. S. Gutierrez, and M. Westfall, Laser-induced melting of a single crystal gold sample by time-resolved ultrafast relativistic electron diffraction, Appl. Phys. Lett. **97,** 063502 (2010).

[189] Bradley J. Siwick, Jason R. Dwyer, Robert E. Jordan, and R. J. Dwayne Miller, Ultrafast electron optics: Propagation dynamics of femtosecond electron packets, J. Appl. Phys. **92,** 1643 (2002).

[190] M. Aidelsburger, F. O. Kirchner, F. Krausz, and P. Baum, Single-electron pulses for ultrafast diffraction, Proc. Natl. Acad. Sci. **107,** 19714 (2010).

[191] Hyun Soon Park, J. Spencer Baskin, Oh-Hoon Kwon, and Ahmed H. Zewail, Atomic-scale imaging in real and energy space developed in ultrafast electron microscopy, Nano Lett. **7,** 2545 (2007).

[192] Hans-Werner Fink, Werner Stocker, and Heinz Schmid, Holography with Low-Energy Electrons, Phys. Rev. Lett. **65,** 1204 (1990).

[193] Erik Quinonez, Jonathan Handali, and Brett Barwick, Femtosecond photoelectron point projection microscope, Rev. Sci. Instrum. **84,** 103710 (2013).

[194] Martin Centurion, Peter Reckenthaeler, Sergei A. Trushin, Ferenc Krausz, and Ernst E. Fill, Picosecond electron deflectometry of optical-field ionized plasmas, Nat. Photonics **2,** 315 (2008).

[195] Junjie Li, Xuan Wang, Zhaoyang Chen, Richard Clinite, Samuel S. Mao, Pengfei Zhu, Zhengming Sheng, Jie Zhang, and Jianming Cao, Ultrafast electron beam imaging of femtosecond laser-induced plasma dynamics, J. Appl. Phys. **107**, 083305 (2010).

[196] C. M. Scoby, R. K. Li, E. Threlkeld, and H. T. O. P. Musumeci, Single-shot 35 fs temporal resolution electron shadowgraphy, Appl. Phys. Lett. **102**, 023506 (2013).

[197] Jan Vogelsang, Jörg Robin, Benedek J. Nagy, Péter Dombi, Daniel Rosenkranz, Manuela Schiek, Petra Groß, and Christoph Lienau, Ultrafast electron emission from a sharp metal nanotaper driven by adiabatic nanofocusing of surface plasmons, Nano Lett. **15**, 4685 (2015).

[198] Björn Piglosiewicz, Slawa Schmidt, Doo Jae Park, Jan Vogelsang, Petra Groß, Cristian Manzoni, Paolo Farinello, Giulio Cerullo, and Christoph Lienau, Carrier-envelope phase effects on the strong-field photoemission of electrons from metallic nanostructures, Nat. Photonics **8**, 37 (2014).

[199] Melanie Müller, Alexander Paarmann, and Ralph Ernstorfer, Femtosecond electrons probing currents and atomic structure in nanomaterials, Nat. Commun. **5**, 5292 (2014).

[200] André Beyer and Armin Gölzhäuser, Low energy electron point source microscopy: Beyond imaging, J. Phys.: Condens. Matter **22**, 343001 (2010).

[201] Jean-Nicolas Longchamp, Conrad Escher, Tatiana Latychevskaia, and Hans-Werner Fink, Low-energy electron holographic imaging of gold nanorods supported by ultraclean graphene, Ultramicroscopy **145**, 80 (2014).

[202] A. R. Bainbridge, C. W. Barlow Myers, and W. A. Bryan, Femtosecond few-to single-electron point-projection microscopy for nanoscale dynamic imaging, Struct. Dyn. **3**, 023612 (2016).

[203] A. A. Mikhailovsky, M. A. Petruska, M. I. Stockman, and V. I. Klimov, Broadband near-field interference spectroscopy of metal nanoparticles using a femtosecond white-light continuum, Opt. Lett. **28**, 1686 (2003).

[204] Achim Hartschuh, Hermeneglido N. Pedrosa, Lukas Novotny, and Todd D. Krauss, Simultaneous fluorescence and Raman scattering from single carbon nanotubes, Science **301**, 1354 (2003).

[205] C. Ropers, C. C. Neacsu, T. Elsaesser, M. Albrecht, M. B. Raschke, and C. Lienau, Grating-coupling of surface plasmons onto metallic tips: A nanoconfined light source, Nano Lett. **7**, 2784 (2007).

[206] Kh.V. Nerkararyan, Superfocusing of a surface polariton in a wedge-like structure, Phys. Lett. A **237**, 103 (1997).

[207] Dmitri K. Gramotnev, David F. P. Pile, Michael W. Vogel, and Xiang Zhang, Local electric field enhancement during nanofocusing of plasmons by a tapered gap, Phys. Rev. B **75**, 035431 (2007).

[208] D. K. Gramotnev and K. C. Vernon, Adiabatic nanofocusing of plasmons by sharp metallic wedges, Appl. Phys. B **86**, 7 (2007).

[209] Kh. Nerkararyan, T. Abrahamyan, E. Janunts, R. Khachatryan, and S. Harutyunyan, Excitation and propagation of surface plasmon polaritons on the gold covered conical tip, Phys. Lett. A **350**, 147 (2006).

[210] Nader A. Issa and Reinhard Guckenberger, Optical nanofocusing on tapered metallic waveguides, Plasmonics **2**, 31 (2007).

[211] Ramani K. Raman, Zhensheng Tao, Tzong-Ru Han, and Chong-Yu Ruan, Ultrafast imaging of photoelectron packets generated from graphite surface, Appl. Phys. Lett. **95**, 181108 (2009).

[212] Yasuaki Okano, Yoichiro Hironaka, Ken-ichi Kondo, and Kazutaka G. Nakamura, Electron imaging of charge-separated field on a copper film induced by femtosecond laser irradiation, Appl. Phys. Lett. **86**, 141501 (2005).

[213] Christoph T. Hebeisen, Germán Sciaini, Maher Harb, Ralph Ernstorfer, Sergei G. Kruglik, and R. J. Dwayne Miller, Direct visualization of charge distributions during femtosecond laser ablation of a Si (100) surface, Phys. Rev. B **78**, 081403 (2008).